

1 **Vertical changes in volatile organic compounds (VOCs) and**  
2 **impacts on photochemical ozone formation**

3 Xiao-Bing Li<sup>1</sup>, Bin Yuan<sup>1,\*</sup>, Yibo Huangfu<sup>1</sup>, Suxia Yang<sup>2</sup>, Xin Song<sup>1</sup>, Jipeng Qi<sup>1</sup>,  
4 Xianjun He<sup>1</sup>, Sihang Wang<sup>1</sup>, Yubin Chen<sup>1</sup>, Qing Yang<sup>1</sup>, Yongxin Song<sup>1</sup>, Yuwen Peng<sup>1</sup>,  
5 Guiqian Tang<sup>3,4</sup>, Jian Gao<sup>5</sup>, Dasa Gu<sup>6</sup>, Min Shao<sup>1</sup>

6 <sup>1</sup> College of Environment and Climate, Institute for Environmental and Climate  
7 Research, Guangdong-Hongkong-Macau Joint Laboratory of Collaborative Innovation  
8 for Environmental Quality, Jinan University, Guangzhou 511443, China

9 <sup>2</sup> Guangzhou Research Institute of Environment Protection Co., Ltd., Guangzhou  
10 510620, China

11 <sup>3</sup> State Key Laboratory of Atmospheric Environment and Extreme Meteorology,  
12 Institute of Atmospheric Physics, Chinese Academy of Sciences, Beijing 100029, China

13 <sup>4</sup> University of Chinese Academy of Sciences, Beijing, 100049, China

14 <sup>5</sup> State Key Laboratory of Environmental Criteria and Risk Assessment, Chinese  
15 Research Academy of Environmental Sciences, Beijing 100012, China

16 <sup>6</sup> Guangdong–Hongkong–Macau Joint Laboratory of Collaborative Innovation for  
17 Environmental Quality and Division of Environment and Sustainability, The Hong  
18 Kong University of Science and Technology, Hong Kong 999077, China

19 \* Corresponding author: Bin Yuan (byuan@jnu.edu.cn)

## 20 **Abstract**

21 Volatile organic compounds (VOCs) play crucial roles in regulating the formation  
22 of tropospheric ozone. However, limited knowledge on the interactions between  
23 vertical VOC variations and photochemical ozone formation in the planetary boundary  
24 layer (PBL) has hindered effective ozone control strategies, especially in large cities.  
25 In this study, we investigated the vertical changes in concentrations, compositions, and  
26 key driving factors of a large suite of VOCs using online gradient measurements taken  
27 from a 325 m tall tower in urban Beijing. The impact of these vertical VOC variations  
28 on photochemical ozone formation were also analyzed using box model simulations.  
29 Our results indicate that VOCs exhibited distinct vertical variation patterns due to their  
30 differences in sources and chemical reactivities, along with the diurnal evolution of the  
31 PBL. During daytime, reactive VOCs (e.g., hydrocarbons) are rapidly oxidized as they  
32 mix upwards, accompanied by the formation and accumulation of oxygenated VOCs  
33 (OVOCs) in the middle and upper layers. In addition, the photochemical formation of  
34 ozone responds positively to changes in both NO<sub>x</sub> and VOCs. As a result, the  
35 production rate of ozone declines with height due to the simultaneous decreases in  
36 concentrations of reactive VOCs and NO<sub>x</sub>, but remains high in the middle and upper  
37 layers. The strong production of ozone aloft is primarily driven by the presence of high  
38 OVOCs concentrations. Therefore, careful consideration should be given to the vertical  
39 variations in both photochemical ozone production rates and formation regimes in the  
40 whole PBL when developing regional ozone control strategies.

## 41 **1 Introduction**

42 Volatile organic compounds (VOCs) are crucial constituents of atmospheric  
43 chemicals (*Li et al., 2022c*) and play important roles in regulating the atmospheric  
44 oxidation capacity and contributing to the photochemical formation of tropospheric  
45 ozone (*Zhao et al., 2022; Yang et al., 2024b*). Ozone is a major air pollutant in urban  
46 environments, with increasing trends reported globally over recent decades (*Fleming et*  
47 *al., 2018; Cooper et al., 2020*), despite stringent measures to control its precursor  
48 emissions (*Wang et al., 2020b; Yeo and Kim, 2021; Li et al., 2022b; Perdignes et al.,*  
49 *2022*). As highlighted in previous studies, reducing emissions of reactive VOCs is key  
50 to controlling ozone pollution at present and in the foreseeable future (*Zhao et al., 2022;*  
51 *Wang et al., 2024*).

52 The primary prerequisite for effective regional ozone pollution control is the  
53 determination of the photochemical ozone formation regime (*Souri et al., 2020; Zhao*  
54 *et al., 2022*), which facilitates the development of reduction schemes for key precursor  
55 emissions (*Ou et al., 2016; Wang et al., 2019*). The main challenges in controlling  
56 ozone pollution stem from the complex compositions of its precursors (e.g., VOCs and  
57 NO<sub>x</sub>) in ambient air (*Guo et al., 2017; Wu et al., 2020; Li et al., 2022c*), as well as the  
58 complicated responses of photochemical ozone formation to changes in these  
59 precursors (*Shao et al., 2021; Perdignes et al., 2022*). Furthermore, the interactions  
60 between vertical variations of ozone precursors and ozone formation remain unclear  
61 (*Tang et al., 2017; Sun et al., 2018; Li et al., 2024*), adding to the complexity of ozone  
62 pollution control.

63 In most cases, the identification of key ozone precursors has been conducted using  
64 ground-level observations (*Qi et al., 2021; Lu et al., 2022*) or compiled source emission  
65 inventories (*Ou et al., 2015; An et al., 2021; Wang et al., 2022b*). While these methods  
66 are undoubtedly helpful in determining key ozone precursors and corresponding  
67 reduction strategies, they often encounter unexpected uncertainties in urban regions.  
68 (*Mo et al., 2018; Mo et al., 2020*). Consequently, ground-level measurements of ozone

69 precursors have been favored to constrain model calculations (*Lu et al., 2012; Wang et*  
70 *al., 2022a; Yang et al., 2022*) or provide empirical evidence for hypothesized theories  
71 (*Hofzumahaus et al., 2009; Wang et al., 2022c*). However, these ground-level  
72 measurements cannot fully characterize atmospheric chemical processes in the entire  
73 planetary boundary layer (PBL) due to strong vertical variations in precursor  
74 concentrations (*Velasco et al., 2008; Li et al., 2018; Sun et al., 2018*).

75 Ambient VOCs, as crucial ozone precursors, are composed of myriad species (*Wu*  
76 *et al., 2020; Gkatzelis et al., 2021; Ye et al., 2021; He et al., 2022*) and serve diverse  
77 functions in photochemical ozone formation (*Vo et al., 2018; Li et al., 2022a; Zhang et*  
78 *al., 2022*). Owing to the impact of variations in emission sources, chemical removal,  
79 advection and convection transport, and secondary formation, the concentration and  
80 composition of VOCs typically display notable vertical variability within the PBL,  
81 especially in urban areas (*Li et al., 2022c*). The ozone formation regime likely  
82 undergoes significant transitions from the ground to the upper boundary layer (*Li et al.,*  
83 *2024; Liu et al., 2024a*). Ozone generated throughout the PBL can influence surface  
84 ozone levels due to enhanced atmospheric vertical mixing during the day. Consequently,  
85 it is imperative to comprehend the vertical variations and principal determinants of  
86 VOCs, as well as their effects on photochemical ozone formation within the PBL.

87 With the rapid development of cities in the recent two decades in China, a large  
88 number of pollution-emitting industries and factories have been relocated from city  
89 centers to alleviate air pollution. Concurrently, there's been a swift increase in the  
90 ownership of electric vehicles (*Guo et al., 2021*). These shifts in energy consumption  
91 have driven the change in concentrations and compositions of VOCs in major cities like  
92 Beijing (*Liu et al., 2024b*), subsequently affecting photochemical ozone formation  
93 (*Wang et al., 2024*). However, the vertical variations and key drivers of VOCs and their  
94 impacts on photochemical ozone formation in the urban PBL remain elusive. A primary  
95 hurdle in studying these vertical changes in photochemical ozone formation is the  
96 scarcity of reliable vertical VOC data (*Dieu Hien et al., 2019; Li et al., 2022c*).  
97 Engaging in vertical profiling of VOCs, ensuring all necessary species represented and

98 obtaining sufficient sample size, is especially challenging in the lower PBL where  
99 atmospheric chemical reactions are most intense (*Benish et al., 2020; Kim et al., 2021*).

100 Previous studies on vertical distributions of photochemical ozone formation in the  
101 PBL have been conducted using measurements of a limited number of VOC species  
102 and samples (*Zhang et al., 2018; Benish et al., 2020; Geng et al., 2020*). In this study,  
103 online gradient measurements of ozone, NO<sub>x</sub>, and a large suit of VOCs were made on  
104 a 325 m tall tower in urban Beijing during the summer of 2021. Additionally, box model  
105 simulations constrained by the gradient measurements were performed to analyze the  
106 vertical variations and key drivers of VOCs as well as their impacts on photochemical  
107 ozone formation.

## 108 **2 Methods and materials**

### 109 **2.1 Description of the site, instrument, and field campaign**

110 The data utilized in this study was derived from an intensive field campaign  
111 conducted at the Beijing Meteorological Tower (BMT: 39°58' N, 116°23' E) between  
112 July 6 and August 4, 2021. The BMT has a height of 325 m and is located in the northern  
113 part of downtown Beijing, positioned between the third and fourth ring roads (Fig. S1).  
114 A vertical observation system, established using long perfluoroalkoxy alkane (PFA)  
115 Teflon tubes (OD: 1/2 in.), was used to make online gradient measurements of ozone,  
116 NO<sub>x</sub>, and a set of VOCs on the BMT. Five specific heights, namely 15, 47, 102, 200,  
117 and 320 m above ground level, were selected to mount the tube inlets, as depicted in  
118 Fig. S3. An additional inlet, situated approximately 5 m above ground level, was  
119 mounted on the rooftop of the observation room that was adjacent to the tower.  
120 Consequently, the vertical observation system totally included a total of six sampling  
121 inlets. The sampling inlet at the 15 m height was not utilized during this field campaign.

122 Filters were installed downstream of the tubing inlets on the tower to remove fine  
123 particles. A rotary vane vacuum pump was used to simultaneously and continuously  
124 draw sample air from the five tubes, ensuring that all tubes were flushed by ambient air

125 to reduce tubing delays of sticky organic compounds (*Pagonis et al., 2017; Liu et al.,*  
126 *2019*). Five critical orifices were employed to control the flow rate of the air stream in  
127 each tubing, resulting in flow rates ranging between 15 and 20 standard liter per minute  
128 (SLPM). Instruments drew sample air from the five tubes sequentially through a Teflon  
129 solenoid valve group at designated time intervals. The switching time intervals of the  
130 Teflon solenoid valve group were set as 4 minutes during this field campaign. The  
131 measurements of trace gases in the first and last 1 minute of a four-minute period were  
132 discarded to eliminate cross interferences between different inlet heights. Detailed  
133 information on the vertical observation system and the assessment of trace gas  
134 measurements through hundreds of meters long PFA tubes has been provided in our  
135 previous works (*Li et al., 2023; Song et al., 2024; Yang et al., 2024a*).

136 Ozone was measured using the ultraviolet photometry method (49i, Thermo Fisher  
137 Scientific Inc., USA). NO, NO<sub>2</sub>, and NO<sub>x</sub> were measured using the chemiluminescence  
138 method (42i, Thermo Fisher Scientific Inc., USA). Gradient measurements of ozone  
139 and NO<sub>x</sub> were conducted at a time resolution of 10 seconds. The photolysis frequencies  
140 of NO<sub>2</sub>, represented by  $j(\text{NO}_2)$ , were measured by a spectrometer (PFS-100, Focused  
141 Photonics Inc., China) situated on the rooftop of the observation room and have a time  
142 resolution of 8 seconds. In situ measurements of meteorological parameters including  
143 wind speed, air temperature, and relative humidity were made at 15 heights between 8  
144 m and 320 m on the BMT with a time resolution of 20 seconds. Planetary boundary  
145 layer height (PBLH) was obtained from the Air Resources Laboratory  
146 (<https://ready.arl.noaa.gov/READYamet.php>, last access: 10 June 2024) and was  
147 linearly interpolated to hourly values based on the initial time resolutions of three hours  
148 (*Li and Fan, 2022*).

149 A high-resolution proton-transfer-reaction quadrupole interface time-of-flight  
150 mass spectrometer (PTR-ToF-MS, Ionicon Analytik, Austria) was employed to measure  
151 VOCs at a time resolution of 10 seconds. The PTR-ToF-MS used both hydronium ion  
152 (H<sub>3</sub>O<sup>+</sup>) (*Yuan et al., 2017; Wu et al., 2020; Li et al., 2022c*) and nitric oxide ion (NO<sup>+</sup>)  
153 (*Wang et al., 2020a*) as reagent ions. These two reagent ions were automatically

154 switched every 60 min for  $\text{H}_3\text{O}^+$  and every 22 min for  $\text{NO}^+$  throughout the campaign.  
155 The PTR-ToF-MS operated at an E/N value of approximately 120 Td in  $\text{H}_3\text{O}^+$  mode  
156 and an E/N value of around 60 Td in  $\text{NO}^+$  mode. Instrument backgrounds were  
157 automatically measured during the last two minutes of each operation mode by passing  
158 ambient air through a platinum catalyst heated to 365 °C. A gas standard containing 39  
159 VOC species was used to calibrate the PTR-ToF-MS daily. Sensitivities for the  
160 remaining species were determined based on reaction kinetics of the PTR-ToF-MS (*Wu*  
161 *et al.*, 2020). Impacts of ambient humidity on the PTR-ToF-MS measurements were  
162 corrected by using humidity-dependence curves of VOCs obtained in our laboratory  
163 (*Wang et al.*, 2020a; *Wu et al.*, 2020). Carbon dioxide ( $\text{CO}_2$  in dry air) and humidity  
164 were measured using a  $\text{CO}_2$  and  $\text{H}_2\text{O}$  gas analyzer (Li-840A, Licor Inc., USA) at a time  
165 resolution of 10 seconds.

166 Gradient measurements of the total OH reactivity (OHR) of atmospheric trace  
167 gases were made using the improved comparative reactivity method (ICRM) developed  
168 by our team (*Wang et al.*, 2021a) from July 28 to 31. In addition, gradient measurements  
169 of carbon monoxide (CO), methane ( $\text{CH}_4$ ),  $\text{CO}_2$ , and  $\text{H}_2\text{O}$  were simultaneously  
170 measured using the cavity ring-down spectroscopy (CRDS) method (G-2401, Picarro  
171 Inc., USA) at a time resolution of 10 seconds from May 15 to June 25. Sulfur dioxide  
172 ( $\text{SO}_2$ ) was measured using the ultraviolet fluorescence method (43i, Thermo Fisher  
173 Scientific Inc., USA) at a time resolution of 10 seconds from June 25 to August 3. The  
174 total OHR of VOCs, denoted by  $\text{OHR}_{\text{VOCs}}$ , can be estimated by excluding those of the  
175 inorganic species (namely ozone,  $\text{NO}_x$ , CO,  $\text{SO}_2$ , and  $\text{CH}_4$ ). It should be noted that  
176 gradient measurements of  $\text{CH}_4$  and CO were not made during July 28-31, and their  
177 average concentrations in daytime (11:00-16:00 LT) between May 15 and June 25 at 5  
178 m were used for all altitudes to calculate  $\text{OHR}_{\text{VOCs}}$ . This method will bring minor  
179 uncertainties due to the minor vertical differences in concentrations of  $\text{CH}_4$  and CO in  
180 daytime (Fig. S4). The OHR of VOCs can also be calculated by summing the products  
181 of their measured concentrations and their reaction rate coefficients with OH radicals,  
182 as formulated in Eq. (1):

$$\text{OHR} = \sum k^i_{\text{OH-R}}[\text{VOC}_i] \quad \text{Eq. (1)}$$

183 where  $k^i_{\text{OH-R}}$  is the reaction rate coefficient of the  $i^{\text{th}}$  VOC species with OH radical  
 184 and  $[\text{VOC}_i]$  is the concentration of the  $i^{\text{th}}$  VOC species.

## 185 2.2 Estimation of NMHC concentrations at the BMT site

186 The PTR-ToF-MS is limited in its ability to measure VOC species with proton  
 187 affinities higher than  $\text{H}_2\text{O}$  ( $691 \text{ kJ mol}^{-1}$ ) when operating in the  $\text{H}_3\text{O}^+$  mode (*Yuan et*  
 188 *al., 2017*). This limitation results in the absence of certain nonmethane hydrocarbons  
 189 (NMHCs), such as alkanes and many alkene species, which play important roles in  
 190 photochemical ozone formation. To obtain a comprehensive understanding of vertical  
 191 variations in concentrations, compositions, and environmental impacts of VOCs, this  
 192 study estimated the vertical profiles of those unmeasured NMHC species based on the  
 193 concentrations of measured VOCs using the PTR-ToF-MS. Detailed information on  
 194 estimation of NMHC concentrations is provided in SI.

## 195 2.3 Box model setup

196 A zero-dimension box model (F0AM) coupled with the Master Chemical  
 197 Mechanism (v3.3.1) (*Wolfe et al., 2016; Yang et al., 2022*) was used to compute the  
 198 production rate of ozone, denoted by  $P(\text{O}_3)$  as formulated in Eq. (2):

$$P(\text{O}_3) = k_{\text{HO}_2+\text{NO}}[\text{HO}_2][\text{NO}] + \sum k^i_{\text{RO}_2+\text{NO}}[\text{R}^i\text{O}_2][\text{NO}] \quad \text{Eq. (2)}$$

$$199 \quad k_{\text{RO}_2+\text{NO}}[\text{RO}_2][\text{NO}]$$

200 where  $[\text{HO}_2]$  and  $[\text{NO}]$  is the concentrations of  $\text{HO}_2$  and  $\text{NO}$ ,  $[\text{R}^i\text{O}_2]$  is the concentration  
 201 of the  $i^{\text{th}}$  organic peroxy radical. The relative incremental reactivity (RIR) of  
 202 photochemical ozone production to changes in different precursors was determined  
 203 using Eq. (3):

$$\text{RIR}(X) = \frac{[P_{\text{O}_x}^S(X) - P_{\text{O}_x}^S(X - \Delta X)]/P_{\text{O}_x}^S(X)}{\Delta S(X)/S(X)} \quad \text{Eq. (3)}$$



204 where X represents ozone precursors,  $P_{O_x}^S(X)$  is the contribution of X to the production  
205 rate of  $O_x$ ,  $\Delta X$  is the amount of change in ozone precursors,  $S(X)$  is the initial  
206 concentration of X. RIR values were used to discern sensitivities of photochemical  
207 ozone formation to changes in precursor gases. A positive RIR(X) value suggests that  
208 an increase in X enhances ozone formation, while a negative RIR value indicates that  
209 an increase in X inhibits ozone formation.

210 Model calculations were constrained by measurements of ozone,  $NO_x$ , CO, a suit  
211 of VOCs, air temperature, and relative humidity. In addition to the measured or  
212 estimated concentrations of NMHCs, nine oxygenated VOC (OVOC) species (Table  
213 S1) measured by PTR-ToF-MS were used to constrain the model calculation. The  
214 model was run in a time-dependent mode with a time resolution of 5 minutes and a  
215 spin-up period of 2 days (Lu et al., 2012; Wang et al., 2022c). The dry deposition  
216 velocity of ozone was set as  $0.27 \text{ cm s}^{-1}$  when calculating  $P(O_3)$  5 m and was zeroed  
217 out when calculating  $P(O_3)$  at other heights.

## 218 **3 Results and discussions**

### 219 **3.1 Temporal and vertical variations in concentrations of trace gases**

220 As shown in Fig. 1, the meteorology in Beijing was characterized by high air  
221 temperature ( $27.3 \pm 2.9 \text{ }^\circ\text{C}$ ), high humidity ( $83.9\% \pm 16.2\%$ ), and gentle winds ( $1.1 \pm 0.4$   
222  $\text{m s}^{-1}$ ) throughout the campaign. The intense solar radiation, elevated air temperature,  
223 and mild winds favored the photochemical formation and accumulation of ozone,  
224 leading to frequent occurrences of ozone pollution episodes. Fig. 1 also presents time  
225 series of mixing ratios of ozone and its selected precursors (namely isoprene, toluene,  
226 monoterpenes, and  $NO_x$ ) along with  $j(NO_2)$  measured at 5 m. The campaign mean  
227 ozone mixing ratio was  $45.6 \pm 25.3 \text{ ppb}$ , but the maximum hourly mean ozone mixing  
228 ratio reached  $129.3 \text{ ppb}$ , indicating strong photochemical reactions in urban Beijing  
229 during the campaign. Surface ozone concentrations exhibited a typical diurnal variation

230 pattern with the maximum occurring at 16:00 LT (Fig. S6), implying its predominant  
231 source from local photochemical production.

232 Isoprene is a typical tracer of biogenic emissions and is also a highly reactive VOC  
233 species (*Atkinson and Arey, 2003*). Isoprene had a campaign mean mixing ratio of  
234  $0.7\pm 0.6$  ppb. The average diurnal profile of isoprene at 5 m has a unimodal pattern with  
235 the maximum occurring at 14:00 LT (Fig. S6), exhibiting strong dependence on solar  
236 radiation. Monoterpenes were also generally recognized as typical tracers of biogenic  
237 emissions (*Gómez et al., 2020*) and have a campaign mean mixing ratio of  $0.3\pm 0.3$  ppb.  
238 The average diurnal profile of monoterpenes was characterized by low mixing ratios in  
239 daytime with two peaks occurring at 05:00 and 20:00 LT, respectively.

240 Toluene and NO<sub>x</sub> are recognized as typical tracers of anthropogenic emissions in  
241 urban regions (*Niu et al., 2017; Li et al., 2022c*), with campaign mean mixing ratios of  
242  $0.7\pm 0.7$  and  $8.1\pm 4.8$  ppb, respectively. The average diurnal profiles of toluene and NO<sub>x</sub>  
243 at 5 m exhibited similar variations with larger values at night than during the day. Based  
244 on the measured concentrations and diurnal variations of ozone and its key precursors  
245 at ground level, it can be inferred that urban Beijing is experiencing severe ozone  
246 pollution, which is predominantly contributed by local photochemical production. As  
247 key ozone precursors, ambient concentrations of VOCs are contributed by the mixture  
248 of anthropogenic and biogenic sources.

249 Fig. 2 shows the average diurnal and vertical variations in mixing ratios of ozone,  
250 NO<sub>x</sub>, Ox (O<sub>3</sub>+NO<sub>2</sub>), and six selected VOC species (three hydrocarbons and three  
251 OVOCs) within the measurement height range of 5-320 m. High mixing ratios of ozone  
252 were observed in the afternoon following the enhancement of solar radiation, which  
253 was consistent with the diurnal change pattern of ozone concentrations at the ground  
254 level. The vertical gradients of ozone mixing ratios were positive throughout the day  
255 but substantially enhanced at night (Fig. 3). The lower ozone mixing ratios near the  
256 surface than aloft were mainly caused by the enhancement of dry deposition and NO  
257 titration (*Brown et al., 2007; Ma et al., 2013; Li et al., 2022b*).

258 NO<sub>x</sub> is a primary pollutant and mainly contributed by vehicular exhausts in urban  
259 regions. In contrast to ozone, NO<sub>x</sub> mixing ratios were low in daytime and exhibited  
260 negative vertical gradients throughout the day, as shown in Figs. 2B and 3A-B. In  
261 nighttime, large amounts of local NO<sub>x</sub> emissions were trapped and accumulated in a  
262 shallow boundary layer (<100 m). NO<sub>x</sub> concentrations rapidly decreased with height  
263 even in the overlying residual layer due to the suppression of turbulence vertical mixing.  
264 With the onset of sunlight, the PBL rapidly expanded due to the surface heating effect.  
265 The accumulated high concentrations of NO<sub>x</sub> in the shallow nocturnal boundary layer  
266 were thereupon diluted and removed by photochemical reactions.

267 Ox is frequently used as a conserved metric to investigate temporal and spatial  
268 variability of ozone by eliminating the NO titration effect. As shown in Fig. 2C, the  
269 mixing ratios of Ox had similar diurnal and vertical variation patterns to those of ozone,  
270 but the vertical gradients of Ox were weaker than those of ozone. This result suggests  
271 that the vertical distribution of NO concentrations played an important role in regulating  
272 the vertical change of ozone concentrations. The enhanced positive gradients of ozone  
273 mixing ratios at night were predominantly due to the strict suppression of turbulence  
274 vertical mixing (*Geyer and Stutz, 2004*). The higher concentrations of ozone aloft are  
275 considered as the residual of the ozone produced in the daytime PBL and have been  
276 recognized as an important reservoir for the enhancement of surface ozone in morning  
277 periods (*Kaser et al., 2017; Li and Fan, 2022; He et al., 2023*).

278 Benzene and toluene demonstrated similar diurnal and vertical variations to NO<sub>x</sub>,  
279 with low concentrations in daytime and high concentrations at night, as shown in Figs.  
280 2D-F and 3A-B. The concentrations of both benzene and toluene decreased with height  
281 throughout the day, confirming their primary emissions from ground-level sources.  
282 However, unlike benzene, the diurnal and vertical variations of toluene were more  
283 pronounced. Isoprene emissions are highly dependent on solar radiation, resulting in its  
284 higher concentrations in the early afternoon compared to other times of the day.  
285 Isoprene mixing ratios also exhibited strong negative vertical gradients below 320 m  
286 throughout the day. In contrast to toluene, isoprene concentrations decreased more

287 rapidly with height in the daytime. For instance, the mixing ratios of isoprene decreased  
288 by approximately 70% from 5 to 320 m in the daytime, while it was only 30% for  
289 toluene.

290 Fig. 3A-B show the average vertical profiles of the NMHCs, normalized to their  
291 respective ground-level concentrations measured by the PTR-ToF-MS in daytime and  
292 nighttime. The normalized mixing ratios of the NMHCs exhibited significantly  
293 differentiated gradients in daytime. In contrast, apart from monoterpenes, the  
294 differences in vertical gradients of the normalized vertical profiles for other NMHCs  
295 were relatively small at night. The differentiated vertical gradients of the NMHCs in  
296 daytime were primarily caused by their intrinsic chemical reactivities, such as reactions  
297 with OH radicals. As shown in Fig. 4, concentration ratios of the NMHC species  
298 between 320 m and 5 m with  $k_{OH}$  values lower than  $2.5 \times 10^{-11} \text{ cm}^3 \text{ molecule}^{-1} \text{ s}^{-1}$   
299 exhibited slight variability and rapidly declined with the further increases in  $k_{OH}$ . The  
300 lower NMHC concentrations at higher altitudes were predominantly caused by the  
301 combined effects of atmospheric diffusion and chemical removal (*Sangiorgi et al.*,  
302 2011).

303 Considering the effects of atmospheric diffusion and chemical removal by  
304 reactions with OH radicals, concentration ratios of NMHC species between 320 m and  
305 5 m in daytime can be estimated using Eq. (4):

$$y = A \times \exp(-k_{OH}[\text{OH}]\Delta t) \quad \text{Eq. (4)}$$

306 where  $y$  represents concentration ratios of the NMHC species between two altitudes,  $A$   
307 represents the effect of atmospheric dilution,  $k_{OH}$  is the reaction rate coefficient of  
308 NMHCs with OH radicals,  $[\text{OH}]$  is the concentration of OH radical,  $\Delta t$  is the  
309 turbulence mixing time scale between the two altitudes. The term  $[\text{OH}]\Delta t$  thus refers  
310 to the exposure of NMHCs to OH radicals between the two altitudes. As shown in Fig.  
311 4, the average concentration ratios of NMHCs between 320 m and 5 m in daytime  
312 during the campaign can be well reproduced using Eq. (4) with the coefficients  $A$  of  
313 0.88 and  $[\text{OH}]\Delta t$  of  $1.0 \times 10^{10} \text{ molecules cm}^{-3} \text{ s}$ . Atmospheric diffusion processes have  
314 same impact on the vertical distributions of all trace gases. The differences in vertical

315 gradients of NMHCs were mainly determined by the differences in their chemical  
316 removal rates without considering influences from advection transport.

317 Methanol, as one of the most abundant OVOC species in the atmosphere, had its  
318 lowest concentrations during daytime and displayed negative vertical gradients  
319 throughout the day, as shown in Fig. 2G. The vertical and diurnal variations of methanol  
320 suggest that its ambient concentrations in urban Beijing were mainly contributed by  
321 local primary emissions. Conversely, formaldehyde and MVK+MACR (the first-  
322 generation oxidation products of isoprene), as the photochemical oxidation products of  
323 NMHCs, had higher concentrations during daytime than at night and exhibited  
324 relatively weak vertical concentration gradients (Fig. 2H-I). This is mainly because  
325 these OVOCs are produced from the oxidation of NMHCs during turbulence vertical  
326 mixing and will accumulate in high altitudes. These phenomena were also observed for  
327 other OVOC species, as shown in Fig. 3.

328 The vertical and diurnal variations in concentrations of ozone, NO<sub>x</sub>, and VOCs  
329 are intricately governed by their sources, chemical reactivities, and the evolution of the  
330 PBL (namely the vertical dilution conditions). A significant accumulation of VOCs in  
331 the shallow nocturnal PBL is subsequently vertically diluted and chemically removed  
332 during daytime, thereby impacting the photochemical formation of ozone within the  
333 daytime PBL. In addition, the observed vertical changes in concentrations of VOCs  
334 imply that they will play distinct roles in contributing to photochemical ozone  
335 formation.

### 336 **3.2 Vertical variations in contributions of VOCs to OHR**

337 During the daytime, VOCs are primarily oxidized by OH radicals and contribute  
338 to the photochemical formation of ozone. To provide an overview on the vertical  
339 variations in contributions of different VOCs to OHR, another 1204 ions measured by  
340 the PTR-ToF-MS and can be quantified were used for analysis. All the VOCs were  
341 classified into three large categories, namely C<sub>x</sub>H<sub>y</sub> (including alkanes, alkenes,  
342 aromatics, and other hydrocarbons; 121 species), OVOCs (C<sub>x</sub>H<sub>y</sub>O<sub>1</sub>, 121 species;

343  $C_xH_yO_2$ , 120 species;  $C_xH_yO_{\geq 3}$ , 256 species), and N/S-containing (653 species), as  
344 shown in Fig.5. Acetylene is included in alkenes.

345 Fig. 5A illustrates that the total mixing ratios of VOCs in daytime exhibited a slight  
346 downward trend from 5 m to 320 m, primarily due to the rapid decrease in mixing ratios  
347 of the  $C_xH_y$  category. The total mixing ratios of the  $C_xH_y$  category decreased from 16.8  
348 to 10.6 ppb from 5 m to 320 m, with alkanes making the largest contribution, followed  
349 by alkenes, aromatics, and other  $C_xH_y$ . Alkanes constituted 58% of the total mixing  
350 ratios of  $C_xH_y$  at 5 m, but this proportion increased to 65% at 320 m. The fractional  
351 contributions of alkenes and aromatics in the total mixing ratios of  $C_xH_y$  slightly  
352 declined from 28% to 22% and from 12% to 10%, respectively, between these two  
353 altitudes. As for OVOCs, the  $C_xH_yO_1$  category was the most abundant among the  
354 measurements, contributing to 52%-58% of the total mixing ratios at the five heights,  
355 followed by the  $C_xH_yO_2$  (8%-10%), and  $C_xH_yO_{\geq 3}$  (2%) categories. The mixing ratios of  
356 the N/S-containing category slightly varied around 2.8 ppb between 5-320 m,  
357 contributed to approximately 6% of the total VOC concentrations.

358 Similar to the vertical variations in concentrations, OHRs of the  $C_xH_y$  category,  
359 denoted by  $OHR_{CH}$ , also rapidly decreased from  $6.9 s^{-1}$  to  $2.5 s^{-1}$  between 5 and 320 m,  
360 accounting for 52%-31% in the total OHRs of VOCs (Fig. 5B). Fractional contributions  
361 of alkenes (40-18%), alkanes (5%), and aromatics (5%-4%) to the total OHRs of VOCs  
362 all exhibited decreasing tendencies from 5 m to 320 m. The total OHRs of alkenes  
363 decreased more quickly from 5 to 320 m than those of alkanes and aromatics. OHRs of  
364 the other  $C_xH_y$  category stabilized at approximately  $0.3 s^{-1}$  below 320 m, exhibiting an  
365 increasing contribution (2%-4%) to the total OHRs of VOCs with the increase in height.  
366 The OHRs of other VOC categories only slightly varied without exhibiting a clear  
367 variation trend from 5 to 320 m during the day. As a result, fractional contributions of  
368 the  $C_xH_yO_1$  (27%-42%),  $C_xH_yO_2$  (12%-18%), and  $C_xH_yO_{\geq 3}$  (5%-7%), and N/S-  
369 containing (2%-4%) categories in the total OHRs of VOCs all increased with height.  
370 The increased contributions of OVOCs and N/S-containing species to the total

371 concentrations and OHRs of VOCs implied that air masses became more aged with the  
372 increase in height.

373 As depicted in Fig. 6A-B, high  $\text{OHR}_{\text{CH}}$  values were mainly constrained in the PBL  
374 and is mainly contributed by biogenic hydrocarbons, specifically isoprene, during  
375 daytime due to their high OH reactivities and enhanced emissions. The fractional  
376 contributions of isoprene in  $\text{OHR}_{\text{CH}}$  decreased rapidly with increasing height (Fig. 7A).  
377 For instance, isoprene accounted for a campaign median fraction of 58% in  $\text{OHR}_{\text{CH}}$  at  
378 5 m in daytime, making it a frequent contributor to photochemical ozone formation in  
379 urban regions. However, this fraction decreased to 38% at 320 m. Therefore, it can be  
380 speculated that the total contributions of hydrocarbons to the total OHRs of VOCs will  
381 also rapidly decline from 320 m to the top of the PBL, which typically ranges between  
382 several hundreds of meters to approximately 2~3 km in daytime (Fig. S7).

383 The total concentrations and OHRs of OVOCs only slightly decreased with the  
384 increase in height below 320 m in daytime, as shown in Fig. 6C-D. This is consistent  
385 with the results of (Wang *et al.*, 2021b), which observed high concentrations of OVOCs  
386 in the upper PBL. Consequently, the ratio of  $\text{OHR}_{\text{OVOC}}$  to  $\text{OHR}_{\text{CH}}$ , denoted by  
387  $\text{OHR}_{\text{OVOC}}/\text{OHR}_{\text{CH}}$ , rapidly increased from 0.87 at 5 m to 2.6 at 320 m (Fig. 7A). This  
388 suggests that OVOCs may play more important roles in regulating the photochemical  
389 ozone formation in the middle and upper layers. To assess their potential roles in  
390 contributing to the photochemical ozone formation throughout the PBL, we calculated  
391 the mean OHRs (MOHR) of different VOC categories in daytime using Eq. (5):

$$\text{MOHR}(X) = \left( \sum ([X]_i + [X]_{i-1})(h_i - h_{i-1})/2 \right) / (320 - 5) \quad \text{Eq. (5)}$$

392 where  $\text{MOHR}(X)$  is the MOHR of the VOC category X,  $[X]_i$  is the concentration of  
393 X at the  $i^{\text{th}}$  altitude (namely 5, 47, 102, 200, and 320 m for  $h_i$ ) above ground level.

394 As shown in Fig. 7B, the campaign median MOHR for isoprene was  $1.7 \text{ s}^{-1}$  and  
395 accounted for 48% of the campaign median MOHR of the  $\text{C}_x\text{H}_y$  category. This fraction  
396 was significantly lower than that of isoprene (57%) in  $\text{OHR}_{\text{CH}}$  at 5 m. In addition, the  
397 campaign median MOHR of the  $\text{C}_x\text{H}_y$  category ( $3.5 \text{ s}^{-1}$ ) was also significantly lower

398 than the  $\text{OHR}_{\text{CH}}$  ( $6.0 \text{ s}^{-1}$ ) at 5 m. By contrast, the campaign median MOHR of OVOCs  
399 ( $4.8 \text{ s}^{-1}$ ) was comparable to that of  $\text{OHR}_{\text{OVOC}}$  ( $4.9 \text{ s}^{-1}$ ) at 5 m. As unsaturated  
400 hydrocarbons, most alkene species are more reactive than alkanes and aromatics  
401 (*Atkinson and Arey, 2003*). As a result, alkenes had dominant contributions to the  
402 MOHR of the  $\text{C}_x\text{H}_y$  category and the  $\text{OHR}_{\text{CH}}$  at 5 m in daytime. As shown in Fig. 7C,  
403 the campaign mean OHRs of alkanes, alkenes, and aromatics at 5 m in daytime were  
404  $0.7$ ,  $5.2$ , and  $0.7 \text{ s}^{-1}$ , respectively, accounting for 10%, 75%, and 10% of the  $\text{OHR}_{\text{CH}}$ .  
405 However, the campaign mean MOHRs of alkanes, alkenes, and aromatics were  $0.5$ ,  $2.7$ ,  
406 and  $0.5 \text{ s}^{-1}$ , respectively, accounting for 12%, 68%, and 12% of the MOHR of NMHC.  
407 We can also expect that the total contributions of alkenes to the MOHR of the  $\text{C}_x\text{H}_y$   
408 category in daytime will significantly decrease if their vertical distributions in the whole  
409 PBL are considered.

410 This study investigated and compared the vertical profiles of measured  $\text{OHR}_{\text{VOCs}}$   
411 and calculated  $\text{OHR}_{\text{CH}}$  during daytime over the period of July 28-31, as shown in Fig.  
412 7D. The campaign median of the measured  $\text{OHR}_{\text{VOCs}}$  exhibited a slow decrease from  
413  $38.4 \text{ s}^{-1}$  at 5 m to  $25.4 \text{ s}^{-1}$  at 320 m. As anticipated, the  $\text{OHR}_{\text{CH}}/\text{OHR}_{\text{VOCs}}$  ratio declined  
414 rapidly from 16% to 7% from 5 to 320 m. It is important to note that the small  
415  $\text{OHR}_{\text{CH}}/\text{OHR}_{\text{VOCs}}$  ratio and its declining trend with the increasing height do not imply  
416 the insignificant roles of hydrocarbons in regulating the secondary pollutant formation  
417 in higher altitudes. The measured concentrations of hydrocarbons are merely the  
418 remnants of chemical reactions. The oxidation products of NMHCs, such as OVOCs  
419 and organic nitrates, formed during vertical mixing in daytime, will continue to  
420 participate in atmospheric chemical reactions.

### 421 **3.3 Vertical variations in photochemical ozone formation**

422 The surface ozone budget is intimately linked to the vertical variations of  
423 photochemical ozone formation throughout the PBL. Previous studies have consistently  
424 reported that the photochemical formation of ozone, encompassing both  $\text{P}(\text{O}_3)$  and  
425 ozone formation regimes (namely the  $\text{NO}_x$ -limited, VOCs-limited, and transition



426 regimes), are highly dependent on the change in its precursors (*Shao et al., 2021; Yang*  
427 *et al., 2022*). Consequently, any changes in the concentrations and compositions of  
428 VOCs and NO<sub>x</sub> within the PBL will inevitably lead to alternations in the vertical  
429 distribution of P(O<sub>3</sub>) and ozone formation regimes (*Tang et al., 2017; Li et al., 2024*).

430 Fig. 8A illustrates the average dependence of P(O<sub>3</sub>) on NO<sub>x</sub> concentrations along  
431 with the normalized probability density (NPD) distribution of NO<sub>x</sub> concentrations at 5  
432 m, 200 m, and 320 m in daytime during the field campaign. At different heights, P(O<sub>3</sub>)  
433 all rapidly increased with the rise in NO<sub>x</sub> until a critical NO<sub>x</sub> mixing ratio was reached,  
434 after which P(O<sub>3</sub>) decreased slowly. The critical NO<sub>x</sub> mixing ratios decreased from  
435 approximately 9.5 ppb at 5 m to 5.0 ppb at 320 m, primarily caused by the decreases in  
436 both NO<sub>x</sub> concentrations and the OHRs of VOCs. As also shown in Fig. 8A, the  
437 majority of the measured NO<sub>x</sub> mixing ratios fall into the transition zone of the P(O<sub>3</sub>)-  
438 NO<sub>x</sub> curves, suggesting that the photochemical ozone formation in Beijing belonged to  
439 the transition regime below 320 m.

440 RIR values were also calculated using the box model results to further elucidate  
441 the sensitivities of photochemical ozone formation to changes in multiple precursors at  
442 different altitudes. As shown in Fig. 8B, positive RIR values were observed for both  
443 NO<sub>x</sub> and various VOC groups at the five heights, further confirming that the  
444 photochemical ozone formation belonged to the transition regime in the lower layer.  
445 RIR values for NO<sub>x</sub> rapidly declined from 5 to 320 m, implying that the photochemical  
446 ozone formation in higher altitudes was more prone to be controlled by the abundance  
447 of VOCs. This is also manifested by the increasing RIR values for both AVOCs and  
448 OVOCs from 5 m to 320 m. RIR values for BVOCs significantly decreased with height  
449 due to their rapid removal by reactions with OH radicals when being vertically mixed.  
450 These results are consistent with the results in section 3.3 that the less reactive AVOCs  
451 and OVOCs are the dominant species in regulating the photochemical formation of  
452 ozone in urban regions aloft.

453 According to the vertical distribution patterns of the photochemical ozone  
454 formation regime, P(O<sub>3</sub>) decreases with increasing height alongside simultaneous

455 declines in concentrations of both NO<sub>x</sub> and VOCs. Fig. 8C presents the average diurnal  
456 and vertical variations in  $P(\text{O}_3)$  calculated by the box model during the campaign. The  
457  $P(\text{O}_3)$  values were higher in daytime and correlated well with  $j(\text{NO}_2)$ .  $P(\text{O}_3)$  decreased  
458 from the ground to 320 m, where it still maintained a relatively high value of  
459 approximately 10 ppb h<sup>-1</sup> at noon. These results highlight that the photochemical  
460 formation of ozone aloft also remained strong compared to those at ground level.  
461 Consequently, the downward transport of ozone from high altitudes, driven by  
462 turbulence mixing, can become significant sources of surface ozone during the day  
463 (*Karl et al., 2023*).

464 Due to the measurement height limitation, the vertical distributions of  $P(\text{O}_3)$  in the  
465 middle and upper parts of the PBL were not determined in this study. As reported by  
466 the work in (*Benish et al., 2020*),  $P(\text{O}_3)$  typically exhibited weak and nearly linear  
467 decline tendencies from 300 m to the top of the PBL during daytime.  $P(\text{O}_3)$  at the PBL  
468 top was approximately half of that at 300 m. Consequently, we can assume that  $P(\text{O}_3)$   
469 decreased linearly from 320 m to the top of the PBL. The integral of  $P(\text{O}_3)$  at different  
470 heights within the PBL can then be estimated using a similar method as described in  
471 Eq. (5).

472 As shown in Fig. 8D, the total amount of ozone photochemically produced below  
473 47 m constituted a mere 6% of the entire PBL. This fractional contribution increased to  
474 approximately 35% at 320 m, further corroborating that the majority of the boundary-  
475 layer ozone was produced in the middle and upper layers. Given the enhancement of  
476 turbulence vertical mixing in daytime, ozone produced at high altitudes becomes a  
477 significant source of surface ozone. This is substantiated by the widespread reports of  
478 strong downward ozone fluxes in the bottom part of the PBL (tens of meters above  
479 ground level) (*Fares et al., 2010; Liu et al., 2021; Karl et al., 2023*). Consequently,  
480 when devising ozone control strategies, particularly in urban regions with intricate  
481 precursor emissions, careful considerations should be given to the vertical variations in  
482 the formation regimes of ozone in the PBL.

## 483 **4 Conclusions**

484 In this study, we investigated the vertical variations, key drivers, and  
485 environmental impacts of VOCs in the PBL using tower-based online gradient  
486 measurements in urban Beijing during the summer of 2021. The diurnal and vertical  
487 variations of various VOC species were strictly regulated by the diurnal evolution of  
488 the PBL. In daytime, reactive NMHC species were rapidly oxidized when they were  
489 mixed upward along with the formation of OVOCs. As a result, OVOC species played  
490 more significant roles in regulating the photochemical ozone formation in urban regions  
491 aloft. The photochemical formation of ozone belongs to the transition regime in the  
492 lower part of the PBL and becomes more sensitive to changes in the concentrations of  
493 AVOCs and OVOCs with increasing height.  $P(O_3)$  exhibited decreasing tendencies  
494 with height but remained very large in high altitudes, likely driven by the high  
495 concentrations of OVOCs and OH radicals. Therefore, careful consideration should be  
496 given to the vertical variations in both  $P(O_3)$  and photochemical ozone formation  
497 regimes in the whole PBL when making regional ozone control strategies.

498 The vertical variations in concentrations and compositions of VOCs significantly  
499 influence the formation of secondary pollutants. Furthermore, vertical changes in  
500 chemical reaction environments (e.g., temperature, humidity, and solar radiation) and  
501 concentrations of other chemicals (e.g., particulate matters,  $NO_x$ , ozone) can also  
502 impact the degradation pathways of VOCs. These factors also affect the formation  
503 pathways and production yields of secondary pollutants. This is particularly crucial for  
504 the highly reactive NMHCs in urban areas with complex anthropogenic emissions and  
505 is expected to be thoroughly elucidated in future studies.

## 506 **Data availability**

507 The observational data used in this study are available from corresponding authors  
508 upon request.

## 509 **Author contributions**

510 BY, XBL, and YH designed the research. XBL, BY, YH, XS, JQ, XH, SW, YC,  
511 QY, YS, YP, GT, JG, and MS contributed to the data collection and data analysis. XBL,  
512 SY, and BY designed and performed the box model simulations. XBL and BY wrote  
513 the paper with contributions from all coauthors. All the coauthors discussed the results  
514 and reviewed the paper.

## 515 **Competing interests**

516 The authors declare that they have no conflict of interest.

## 517 **Acknowledgments**

518 The authors would like to thank the personnel who participated in data collection,  
519 instrument maintenance, and logistic support during the field campaign.

## 520 **Financial support**

521 This work was financially supported by the National Key R&D Plan of China  
522 (grant nos. 2023YFC3706103, 2023YFC3706201, 2023YFC3710900, and  
523 2022YFC3700604) and the National Natural Science Foundation of China (grant nos.  
524 42121004, 42275103, 42205094, 42230701, 42305095, and 42475107). This work was  
525 also supported by the Guangdong Basic and Applied Basic Research Foundation (grant  
526 no. 2024A1515011570) and Guangzhou Basic and Applied Basic Research Foundation  
527 (grant no. 2024A04J3958).

## 528 **References**

529 An, J., Huang, Y., Huang, C., Wang, X., Yan, R., Wang, Q., Wang, H., Jing, S., Zhang,  
530 Y., Liu, Y., Chen, Y., Xu, C., Qiao, L., Zhou, M., Zhu, S., Hu, Q., Lu, J., and Chen, C.:  
531 Emission inventory of air pollutants and chemical speciation for specific anthropogenic  
532 sources based on local measurements in the Yangtze River Delta region, China, *Atmos.*  
533 *Chem. Phys.*, 21, 2003-2025, <https://doi.org/10.5194/acp-21-2003-2021> 2021.  
534 Atkinson, R., and Arey, J.: Atmospheric Degradation of Volatile Organic Compounds,  
535 *Chem Rev*, 103, 4605-4638, <https://doi.org/10.1021/cr0206420> 2003.

536 Benish, S. E., He, H., Ren, X., Roberts, S. J., Salawitch, R. J., Li, Z., Wang, F., Wang,  
537 Y., Zhang, F., Shao, M., Lu, S., and Dickerson, R. R.: Measurement report: Aircraft  
538 observations of ozone, nitrogen oxides, and volatile organic compounds over Hebei  
539 Province, China, *Atmos. Chem. Phys.*, 20, 14523-14545,[https://doi.org/10.5194/acp-](https://doi.org/10.5194/acp-20-14523-2020)  
540 [20-14523-2020](https://doi.org/10.5194/acp-20-14523-2020) 2020.

541 Brown, S. S., Dubé, W. P., Osthoff, H. D., Wolfe, D. E., Angevine, W. M., and  
542 Ravishankara, A. R.: High resolution vertical distributions of NO<sub>3</sub> and N<sub>2</sub>O<sub>5</sub> through  
543 the nocturnal boundary layer, *Atmos. Chem. Phys.*, 7, 139-149,[10.5194/acp-7-139-](https://doi.org/10.5194/acp-7-139-2007)  
544 [2007](https://doi.org/10.5194/acp-7-139-2007) 2007.

545 Cooper, O. R., Schultz, M. G., Schroeder, S., Chang, K.-L., Gaudel, A., Benitez, G. C.,  
546 Cuevas, E., Froehlich, M., Galbally, I. E., Molloy, S., Kubistin, D., Lu, X., McClure-  
547 Begley, A., Nedelec, P., O'Brien, J., Oltmans, S. J., Petropavlovskikh, I., Ries, L., Senik,  
548 I., Sjoeborg, K., Solberg, S., Spain, G. T., Spangl, W., Steinbacher, M., Tarasick, D.,  
549 Thouret, V., and Xu, X.: Multi-decadal surface ozone trends at globally distributed  
550 remote locations, *Elementa-Science of the Anthropocene*, 8,<https://doi.org/10.1525/elementa.420>  
551 [2020](https://doi.org/10.1525/elementa.420).

552 Dieu Hien, V. T., Lin, C., Thanh, V. C., Kim Oanh, N. T., Thanh, B. X., Weng, C.-E.,  
553 Yuan, C.-S., and Rene, E. R.: An overview of the development of vertical sampling  
554 technologies for ambient volatile organic compounds (VOCs), *J Environ Manage*, 247,  
555 [401-412,https://doi.org/10.1016/j.jenvman.2019.06.090](https://doi.org/10.1016/j.jenvman.2019.06.090) 2019.

556 Fares, S., McKay, M., Holzinger, R., and Goldstein, A. H.: Ozone fluxes in a *Pinus*  
557 *ponderosa* ecosystem are dominated by non-stomatal processes: Evidence from long-  
558 term continuous measurements, *Agr Forest Meteorol*, 150, 420-  
559 [431,https://doi.org/10.1016/j.agrformet.2010.01.007](https://doi.org/10.1016/j.agrformet.2010.01.007) 2010.

560 Fleming, Z. L., Doherty, R. M., von Schneidmesser, E., Malley, C. S., Cooper, O. R.,  
561 Pinto, J. P., Colette, A., Xu, X., Simpson, D., Schultz, M. G., Lefohn, A. S., Hamad, S.,  
562 Moolla, R., Solberg, S., and Feng, Z.: Tropospheric Ozone Assessment Report: Present-  
563 day ozone distribution and trends relevant to human health, *Elementa-Science of the*  
564 *Anthropocene*, 6,[10.1525/elementa.273](https://doi.org/10.1525/elementa.273) 2018.

565 Geng, C., Wang, J., Yin, B., Zhao, R., Li, P., Yang, W., Xiao, Z., Li, S., Li, K., and Bai,  
566 Z.: Vertical distribution of volatile organic compounds conducted by tethered balloon  
567 in the Beijing-Tianjin-Hebei region of China, *Journal of Environmental Sciences*, 95,  
568 [121-129,https://doi.org/10.1016/j.jes.2020.03.026](https://doi.org/10.1016/j.jes.2020.03.026) 2020.

569 Geyer, A., and Stutz, J.: Vertical profiles of NO<sub>3</sub>, N<sub>2</sub>O<sub>5</sub>, O<sub>3</sub>, and NO<sub>x</sub> in the nocturnal  
570 boundary layer: 2. Model studies on the altitude dependence of composition and  
571 chemistry, *Journal of Geophysical Research: Atmospheres*,  
572 [109,https://doi.org/10.1029/2003jd004211](https://doi.org/10.1029/2003jd004211) 2004.

573 Gkatzelis, G. I., Coggon, M. M., McDonald, B. C., Peischl, J., Gilman, J. B., Aikin, K.  
574 C., Robinson, M. A., Canonaco, F., Prevot, A. S. H., Trainer, M., and Warneke, C.:  
575 Observations Confirm that Volatile Chemical Products Are a Major Source of  
576 Petrochemical Emissions in U.S. Cities, *Environ Sci Technol*, 55, 4332-  
577 [4343,10.1021/acs.est.0c05471](https://doi.org/10.1021/acs.est.0c05471) 2021.

578 Gómez, M. C., Durana, N., García, J. A., de Blas, M., Sáez de Cámara, E., García-Ruiz,  
579 E., Gangoiti, G., Torre-Pascual, E., and Iza, J.: Long-term measurement of biogenic

580 volatile organic compounds in a rural background area: Contribution to ozone  
581 formation, *Atmos Environ*, 224,  
582 117315,<https://doi.org/10.1016/j.atmosenv.2020.117315> 2020.

583 Guo, H., Ling, Z. H., Cheng, H. R., Simpson, I. J., Lyu, X. P., Wang, X. M., Shao, M.,  
584 Lu, H. X., Ayoko, G., Zhang, Y. L., Saunders, S. M., Lam, S. H. M., Wang, J. L., and  
585 Blake, D. R.: Tropospheric volatile organic compounds in China, *Sci Total Environ*,  
586 574, 1021-1043,<https://doi.org/10.1016/j.scitotenv.2016.09.116> 2017.

587 Guo, J.-X., Zeng, Y., Zhu, K., and Tan, X.: Vehicle mix evaluation in Beijing's  
588 passenger-car sector: From air pollution control perspective, *Sci Total Environ*, 785,  
589 147264,<https://doi.org/10.1016/j.scitotenv.2021.147264> 2021.

590 He, G., He, C., Wang, H., Lu, X., Pei, C., Qiu, X., Liu, C., Wang, Y., Liu, N., Zhang,  
591 J., Lei, L., Liu, Y., Wang, H., Deng, T., Fan, Q., and Fan, S.: Nighttime ozone in the  
592 lower boundary layer: insights from 3-year tower-based measurements in South China  
593 and regional air quality modeling, *Atmos. Chem. Phys.*, 23, 13107-13124,[10.5194/acp-](https://doi.org/10.5194/acp-23-13107-2023)  
594 [23-13107-2023](https://doi.org/10.5194/acp-23-13107-2023) 2023.

595 He, X., Yuan, B., Wu, C., Wang, S., Wang, C., Huangfu, Y., Qi, J., Ma, N., Xu, W.,  
596 Wang, M., Chen, W., Su, H., Cheng, Y., and Shao, M.: Volatile organic compounds in  
597 wintertime North China Plain: Insights from measurements of proton transfer reaction  
598 time-of-flight mass spectrometer (PTR-ToF-MS), *J Environ Sci (China)*, 114, 98-  
599 114,[10.1016/j.jes.2021.08.010](https://doi.org/10.1016/j.jes.2021.08.010) 2022.

600 Hofzumahaus, A., Rohrer, F., Lu, K., Bohn, B., Brauers, T., Chang, C.-C., Fuchs, H.,  
601 Holland, F., Kita, K., Kondo, Y., Li, X., Lou, S., Shao, M., Zeng, L., Wahner, A., and  
602 Zhang, Y.: Amplified Trace Gas Removal in the Troposphere, *Science*, 324, 1702-  
603 1704,[doi:10.1126/science.1164566](https://doi.org/10.1126/science.1164566) 2009.

604 Karl, T., Lamprecht, C., Graus, M., Cede, A., Tiefengraber, M., Vila-Guerau de  
605 Arellano, J., Gurarie, D., and Lenschow, D.: High urban NO<sub>x</sub> triggers a substantial  
606 chemical downward flux of ozone, *Science Advances*, 9,  
607 eadd2365,[doi:10.1126/sciadv.add2365](https://doi.org/10.1126/sciadv.add2365) 2023.

608 Kaser, L., Patton, E. G., Pfister, G. G., Weinheimer, A. J., Montzka, D. D., Flocke, F.,  
609 Thompson, A. M., Stauffer, R. M., and Halliday, H. S.: The effect of entrainment  
610 through atmospheric boundary layer growth on observed and modeled surface ozone in  
611 the Colorado Front Range, *Journal of Geophysical Research: Atmospheres*, 122, 6075-  
612 6093,[10.1002/2016jd026245](https://doi.org/10.1002/2016jd026245) 2017.

613 Kim, S., Seco, R., Gu, D., Sanchez, D., Jeong, D., Guenther, A. B., Lee, Y., Mak, J. E.,  
614 Su, L., Kim, D. B., Lee, Y., Ahn, J.-Y., McGee, T., Sullivan, J., Long, R., Brune, W.  
615 H., Thames, A., Wisthaler, A., Mueller, M., Mikoviny, T., Weinheimer, A., Yang, M.,  
616 Woo, J.-H., Kim, S., and Park, H.: The role of a suburban forest in controlling vertical  
617 trace gas and OH reactivity distributions - a case study for the Seoul metropolitan area,  
618 *Faraday Discuss*, 226, 537-550,[10.1039/d0fd00081g](https://doi.org/10.1039/d0fd00081g) 2021.

619 Li, C., Liu, Y., Cheng, B., Zhang, Y., Liu, X., Qu, Y., An, J., Kong, L., Zhang, Y.,  
620 Zhang, C., Tan, Q., and Feng, M.: A comprehensive investigation on volatile organic  
621 compounds (VOCs) in 2018 in Beijing, China: Characteristics, sources and behaviours  
622 in response to O<sub>3</sub> formation, *Sci Total Environ*, 806,  
623 150247,<https://doi.org/10.1016/j.scitotenv.2021.150247> 2022a.

624 Li, X.-B., Wang, D., Lu, Q.-C., Peng, Z.-R., Fu, Q., Hu, X.-M., Huo, J., Xiu, G., Li, B.,  
625 Li, C., Wang, D.-S., and Wang, H.: Three-dimensional analysis of ozone and PM<sub>2.5</sub>  
626 distributions obtained by observations of tethered balloon and unmanned aerial vehicle  
627 in Shanghai, China, *Stoch Env Res Risk A*, 32, 1189-  
628 1203,<https://doi.org/10.1007/s00477-018-1524-2> 2018.

629 Li, X.-B., and Fan, G.: Interannual variations, sources, and health impacts of the  
630 springtime ozone in Shanghai, *Environ Pollut*, 306,  
631 119458,<https://doi.org/10.1016/j.envpol.2022.119458> 2022.

632 Li, X.-B., Yuan, B., Parrish, D. D., Chen, D., Song, Y., Yang, S., Liu, Z., and Shao, M.:  
633 Long-term trend of ozone in southern China reveals future mitigation strategy for air  
634 pollution, *Atmos Environ*, 269, 118869,[10.1016/j.atmosenv.2021.118869](https://doi.org/10.1016/j.atmosenv.2021.118869) 2022b.

635 Li, X.-B., Yuan, B., Wang, S., Wang, C., Lan, J., Liu, Z., Song, Y., He, X., Huangfu,  
636 Y., Pei, C., Cheng, P., Yang, S., Qi, J., Wu, C., Huang, S., You, Y., Chang, M., Zheng,  
637 H., Yang, W., Wang, X., and Shao, M.: Variations and sources of volatile organic  
638 compounds (VOCs) in urban region: insights from measurements on a tall tower,  
639 *Atmos. Chem. Phys.*, 22, 10567-10587,[10.5194/acp-22-10567-2022](https://doi.org/10.5194/acp-22-10567-2022) 2022c.

640 Li, X.-B., Zhang, C., Liu, A., Yuan, B., Yang, H., Liu, C., Wang, S., Huangfu, Y., Qi,  
641 J., Liu, Z., He, X., Song, X., Chen, Y., Peng, Y., Zhang, X., Zheng, E., Yang, L., Yang,  
642 Q., Qin, G., Zhou, J., and Shao, M.: Assessment of long tubing in measuring  
643 atmospheric trace gases: applications on tall towers, *Environmental Science:  
644 Atmospheres*, 3, 506-520,[10.1039/d2ea00110a](https://doi.org/10.1039/d2ea00110a) 2023.

645 Li, X., Wang, W., Yang, S., Cheng, Y., Zeng, L., Yu, X., Lu, S., Liu, Y., Hu, M., Xie,  
646 S., Huang, X., Zhou, J., Shi, L., Xu, H., Lin, S., Liu, H., Feng, M., Song, D., Tan, Q.,  
647 and Zhang, Y.: Ozone sensitivity regimes vary at different heights in the planetary  
648 boundary layer, *Sci Total Environ*, 944,  
649 173712,<https://doi.org/10.1016/j.scitotenv.2024.173712> 2024.

650 Liu, X., Deming, B., Pagonis, D., Day, D. A., Palm, B. B., Talukdar, R., Roberts, J. M.,  
651 Veres, P. R., Krechmer, J. E., Thornton, J. A., de Gouw, J. A., Ziemann, P. J., and  
652 Jimenez, J. L.: Effects of gas-wall interactions on measurements of semivolatile  
653 compounds and small polar molecules, *Atmos. Meas. Tech.*, 12, 3137-  
654 3149,[10.5194/amt-12-3137-2019](https://doi.org/10.5194/amt-12-3137-2019) 2019.

655 Liu, Y., Tang, G., Wang, Y., Cheng, M., Gao, J., and Wang, Y.: Spatiotemporal  
656 differences in tropospheric ozone sensitivity and the impact of “dual carbon” goal,  
657 *Science Bulletin*, 69, 422-425,<https://doi.org/10.1016/j.scib.2023.12.026> 2024a.

658 Liu, Y., Yin, S., Zhang, S., Ma, W., Zhang, X., Qiu, P., Li, C., Wang, G., Hou, D.,  
659 Zhang, X., An, J., Sun, Y., Li, J., Zhang, Z., Chen, J., Tian, H., Liu, X., and Liu, L.:  
660 Drivers and impacts of decreasing concentrations of atmospheric volatile organic  
661 compounds (VOCs) in Beijing during 2016–2020, *Sci Total Environ*, 906,  
662 167847,<https://doi.org/10.1016/j.scitotenv.2023.167847> 2024b.

663 Liu, Z., Pan, Y., Song, T., Hu, B., Wang, L., and Wang, Y.: Eddy covariance  
664 measurements of ozone flux above and below a southern subtropical forest canopy, *Sci  
665 Total Environ*, 791, 148338,<https://doi.org/10.1016/j.scitotenv.2021.148338> 2021.

666 Lu, K. D., Rohrer, F., Holland, F., Fuchs, H., Bohn, B., Brauers, T., Chang, C. C.,  
667 Häseler, R., Hu, M., Kita, K., Kondo, Y., Li, X., Lou, S. R., Nehr, S., Shao, M., Zeng,

668 L. M., Wahner, A., Zhang, Y. H., and Hofzumahaus, A.: Observation and modelling of  
669 OH and HO<sub>2</sub> concentrations in the Pearl River Delta 2006: a missing OH source in a  
670 VOC rich atmosphere, *Atmos. Chem. Phys.*, 12, 1541-1569,10.5194/acp-12-1541-2012  
671 2012.

672 Lu, Y., Pang, X., Lyu, Y., Li, J., Xing, B., Chen, J., Mao, Y., Shang, Q., and Wu, H.:  
673 Characteristics and sources analysis of ambient volatile organic compounds in a typical  
674 industrial park: Implications for ozone formation in 2022 Asian Games, *Sci Total*  
675 *Environ*, 848, 157746,<https://doi.org/10.1016/j.scitotenv.2022.157746> 2022.

676 Ma, Z., Xu, H., Meng, W., Zhang, X., Xu, J., Liu, Q., and Wang, Y.: Vertical ozone  
677 characteristics in urban boundary layer in Beijing, *Environ Monit Assess*, 185, 5449-  
678 5460,10.1007/s10661-012-2958-5 2013.

679 Mo, Z., Shao, M., Wang, W., Liu, Y., Wang, M., and Lu, S.: Evaluation of biogenic  
680 isoprene emissions and their contribution to ozone formation by ground-based  
681 measurements in Beijing, China, *Sci Total Environ*, 627, 1485-  
682 1494,<https://doi.org/10.1016/j.scitotenv.2018.01.336> 2018.

683 Mo, Z., Huang, S., Yuan, B., Pei, C., Song, Q., Qi, J., Wang, M., Wang, B., Wang, C.,  
684 Li, M., Zhang, Q., and Shao, M.: Deriving emission fluxes of volatile organic  
685 compounds from tower observation in the Pearl River Delta, China, *Sci Total Environ*,  
686 741, 139763,<https://doi.org/10.1016/j.scitotenv.2020.139763> 2020.

687 Niu, H., Li, K., Chu, B., Su, W., and Li, J.: Heterogeneous Reactions between Toluene  
688 and NO<sub>2</sub> on Mineral Particles under Simulated Atmospheric Conditions, *Environ Sci*  
689 *Technol*, 51, 9596-9604,<https://doi.org/10.1021/acs.est.7b00194> 2017.

690 Ou, J., Zheng, J., Li, R., Huang, X., Zhong, Z., Zhong, L., and Lin, H.: Speciated OVOC  
691 and VOC emission inventories and their implications for reactivity-based ozone control  
692 strategy in the Pearl River Delta region, China, *Sci Total Environ*, 530-531, 393-  
693 402,<https://doi.org/10.1016/j.scitotenv.2015.05.062> 2015.

694 Ou, J., Yuan, Z., Zheng, J., Huang, Z., Shao, M., Li, Z., Huang, X., Guo, H., and Louie,  
695 P. K. K.: Ambient Ozone Control in a Photochemically Active Region: Short-Term  
696 Despiking or Long-Term Attainment?, *Environ Sci Technol*, 50, 5720-  
697 5728,<https://doi.org/10.1021/acs.est.6b00345> 2016.

698 Pagonis, D., Krechmer, J. E., de Gouw, J., Jimenez, J. L., and Ziemann, P. J.: Effects  
699 of gas-wall partitioning in Teflon tubing and instrumentation on time-resolved  
700 measurements of gas-phase organic compounds, *Atmos. Meas. Tech.*, 10, 4687-  
701 4696,10.5194/amt-10-4687-2017 2017.

702 Perdignes, B. C., Lee, S., Cohen, R. C., Park, J.-H., and Min, K.-E.: Two Decades of  
703 Changes in Summertime Ozone Production in California's South Coast Air Basin,  
704 *Environ Sci Technol*, 56, 10586-10595,10.1021/acs.est.2c01026 2022.

705 Qi, J., Mo, Z., Yuan, B., Huang, S., Huangfu, Y., Wang, Z., Li, X., Yang, S., Wang,  
706 W., Zhao, Y., Wang, X., Wang, W., Liu, K., and Shao, M.: An observation approach in  
707 evaluation of ozone production to precursor changes during the COVID-19 lockdown,  
708 *Atmos Environ*, 262, 118618,<https://doi.org/10.1016/j.atmosenv.2021.118618> 2021.

709 Sangiorgi, G., Ferrero, L., Perrone, M. G., Bolzacchini, E., Duane, M., and Larsen, B.  
710 R.: Vertical distribution of hydrocarbons in the low troposphere below and above the



711 mixing height: Tethered balloon measurements in Milan, Italy, *Environ Pollut*, 159,  
712 3545-3552, <https://doi.org/10.1016/j.envpol.2011.08.012> 2011.

713 Shao, M., Wang, W., Yuan, B., Parrish, D. D., Li, X., Lu, K., Wu, L., Wang, X., Mo,  
714 Z., Yang, S., Peng, Y., Kuang, Y., Chen, W., Hu, M., Zeng, L., Su, H., Cheng, Y.,  
715 Zheng, J., and Zhang, Y.: Quantifying the role of PM<sub>2.5</sub> dropping in variations of  
716 ground-level ozone: Inter-comparison between Beijing and Los Angeles, *Sci Total*  
717 *Environ*, 147712, <https://doi.org/10.1016/j.scitotenv.2021.147712> 2021.

718 Song, X., Li, X.-B., Yuan, B., He, X., Chen, Y., Wang, S., Huangfu, Y., Peng, Y.,  
719 Zhang, C., Liu, A., Yang, H., Liu, C., Li, J., and Shao, M.: Elucidating key factors in  
720 regulating budgets of ozone and its precursors in atmospheric boundary layer, *npj*  
721 *Climate and Atmospheric Science*, 7, 262, 10.1038/s41612-024-00818-8 2024.

722 Souri, A. H., Nowlan, C. R., Wolfe, G. M., Lamsal, L. N., Chan Miller, C. E., Abad, G.  
723 G., Janz, S. J., Fried, A., Blake, D. R., Weinheimer, A. J., Diskin, G. S., Liu, X., and  
724 Chance, K.: Revisiting the effectiveness of HCHO/NO<sub>2</sub> ratios for inferring ozone  
725 sensitivity to its precursors using high resolution airborne remote sensing observations  
726 in a high ozone episode during the KORUS-AQ campaign, *Atmos Environ*, 224,  
727 117341, <https://doi.org/10.1016/j.atmosenv.2020.117341> 2020.

728 Sun, J., Wang, Y., Wu, F., Tang, G., Wang, L., Wang, Y., and Yang, Y.: Vertical  
729 characteristics of VOCs in the lower troposphere over the North China Plain during  
730 pollution periods, *Environ Pollut*, 236, 907-  
731 915, <https://doi.org/10.1016/j.envpol.2017.10.051> 2018.

732 Tang, G., Zhu, X., Xin, J., Hu, B., Song, T., Sun, Y., Zhang, J., Wang, L., Cheng, M.,  
733 Chao, N., Kong, L., Li, X., and Wang, Y.: Modelling study of boundary-layer ozone  
734 over northern China - Part I: Ozone budget in summer, *Atmos Res*, 187, 128-  
735 137, <https://doi.org/10.1016/j.atmosres.2016.10.017> 2017.

736 Velasco, E., Marquez, C., Bueno, E., Bernabe, R. M., Sanchez, A., Fentanes, O.,  
737 Wohnschimmel, H., Cardenas, B., Kamilla, A., Wakamatsu, S., and Molina, L. T.:  
738 Vertical distribution of ozone and VOCs in the low boundary layer of Mexico City,  
739 *Atmos. Chem. Phys.*, 8, 3061-3079, <https://doi.org/10.5194/acp-8-3061-2008> 2008.

740 Vo, T.-D.-H., Lin, C., Weng, C.-E., Yuan, C.-S., Lee, C.-W., Hung, C.-H., Bui, X.-T.,  
741 Lo, K.-C., and Lin, J.-X.: Vertical stratification of volatile organic compounds and their  
742 photochemical product formation potential in an industrial urban area, *J Environ*  
743 *Manage*, 217, 327-336, <https://doi.org/10.1016/j.jenvman.2018.03.101> 2018.

744 Wang, C., Yuan, B., Wu, C., Wang, S., Qi, J., Wang, B., Wang, Z., Hu, W., Chen, W.,  
745 Ye, C., Wang, W., Sun, Y., Wang, C., Huang, S., Song, W., Wang, X., Yang, S., Zhang,  
746 S., Xu, W., Ma, N., Zhang, Z., Jiang, B., Su, H., Cheng, Y., Wang, X., and Shao, M.:  
747 Measurements of higher alkanes using NO<sup>+</sup> chemical ionization in PTR-ToF-MS:  
748 important contributions of higher alkanes to secondary organic aerosols in China,  
749 *Atmos. Chem. Phys.*, 20, 14123-14138, <https://doi.org/10.5194/acp-20-14123-2020>  
750 2020a.

751 Wang, H., Ma, X., Tan, Z., Wang, H., Chen, X., Chen, S., Gao, Y., Liu, Y., Liu, Y.,  
752 Yang, X., Yuan, B., Zeng, L., Huang, C., Lu, K., and Zhang, Y.: Anthropogenic  
753 monoterpenes aggravating ozone pollution, *Natl Sci Rev*, 9,  
754 nwac103, 10.1093/nsr/nwac103 2022a.

755 Wang, N., Lyu, X., Deng, X., Huang, X., Jiang, F., and Ding, A.: Aggravating O<sub>3</sub>  
756 pollution due to NO<sub>x</sub> emission control in eastern China, *Sci Total Environ*, 677, 732-  
757 744,<https://doi.org/10.1016/j.scitotenv.2019.04.388> 2019.

758 Wang, N., Huang, X., Xu, J., Wang, T., Tan, Z.-m., and Ding, A.: Typhoon-boosted  
759 biogenic emission aggravates cross-regional ozone pollution in China, *Science*  
760 *Advances*, 8, eabl6166,doi:10.1126/sciadv.abl6166 2022b.

761 Wang, W., Qi, J., Zhou, J., Yuan, B., Peng, Y., Wang, S., Yang, S., Williams, J., Sinha,  
762 V., and Shao, M.: The improved comparative reactivity method (ICRM): measurements  
763 of OH reactivity under high-NO<sub>x</sub> conditions in ambient air, *Atmos. Meas. Tech.*, 14,  
764 2285-2298,10.5194/amt-14-2285-2021 2021a.

765 Wang, W., Yuan, B., Peng, Y., Su, H., Cheng, Y., Yang, S., Wu, C., Qi, J., Bao, F.,  
766 Huangfu, Y., Wang, C., Ye, C., Wang, Z., Wang, B., Wang, X., Song, W., Hu, W.,  
767 Cheng, P., Zhu, M., Zheng, J., and Shao, M.: Direct observations indicate  
768 photodegradable oxygenated volatile organic compounds (OVOCs) as larger  
769 contributors to radicals and ozone production in the atmosphere, *Atmos. Chem. Phys.*,  
770 22, 4117-4128,10.5194/acp-22-4117-2022 2022c.

771 Wang, W., Li, X., Cheng, Y., Parrish, D. D., Ni, R., Tan, Z., Liu, Y., Lu, S., Wu, Y.,  
772 Chen, S., Lu, K., Hu, M., Zeng, L., Shao, M., Huang, C., Tian, X., Leung, K. M., Chen,  
773 L., Fan, M., Zhang, Q., Rohrer, F., Wahner, A., Pöschl, U., Su, H., and Zhang, Y.:  
774 Ozone pollution mitigation strategy informed by long-term trends of atmospheric  
775 oxidation capacity, *Nature Geoscience*, 17, 20-25,10.1038/s41561-023-01334-9 2024.

776 Wang, Y., Wang, Y., Tang, G., Yang, Y., Li, X., Yao, D., Wu, S., Kang, Y., Wang, M.,  
777 and Wang, Y.: High gaseous carbonyl concentrations in the upper boundary layer in  
778 Shijiazhuang, China, *Sci Total Environ*, 799,  
779 149438,<https://doi.org/10.1016/j.scitotenv.2021.149438> 2021b.

780 Wang, Y. H., Gao, W. K., Wang, S., Song, T., Gong, Z. Y., Ji, D. S., Wang, L. L., Liu,  
781 Z. R., Tang, G. Q., Huo, Y. F., Tian, S. L., Li, J. Y., Li, M. G., Yang, Y., Chu, B. W.,  
782 Petaja, T., Kerminen, V. M., He, H., Hao, J. M., Kulmala, M., Wang, Y. S., and Zhang,  
783 Y. H.: Contrasting trends of PM<sub>2.5</sub> and surface-ozone concentrations in China from  
784 2013 to 2017, *National Science Review*, 7, 1331-  
785 1339,<https://doi.org/10.1093/nsr/nwaa032> 2020b.

786 Wolfe, G. M., Marvin, M. R., Roberts, S. J., Travis, K. R., and Liao, J.: The Framework  
787 for 0-D Atmospheric Modeling (F0AM) v3.1, *Geoscientific Model Development*, 9,  
788 3309-3319,10.5194/gmd-9-3309-2016 2016.

789 Wu, C., Wang, C., Wang, S., Wang, W., Yuan, B., Qi, J., Wang, B., Wang, H., Wang,  
790 C., Song, W., Wang, X., Hu, W., Lou, S., Ye, C., Peng, Y., Wang, Z., Huangfu, Y., Xie,  
791 Y., Zhu, M., Zheng, J., Wang, X., Jiang, B., Zhang, Z., and Shao, M.: Measurement  
792 report: Important contributions of oxygenated compounds to emissions and chemistry  
793 of volatile organic compounds in urban air, *Atmos. Chem. Phys.*, 20, 14769-  
794 14785,<https://doi.org/10.5194/acp-20-14769-2020> 2020.

795 Yang, Q., Li, X. B., Yuan, B., Zhang, X., Huangfu, Y., Yang, L., He, X., Qi, J., and  
796 Shao, M.: Measurement report: Enhanced photochemical formation of formic and  
797 isocyanic acids in urban regions aloft – insights from tower-based online gradient  
798 measurements, *Atmos. Chem. Phys.*, 24, 6865-6882,10.5194/acp-24-6865-2024 2024a.

799 Yang, S., Yuan, B., Peng, Y., Huang, S., Chen, W., Hu, W., Pei, C., Zhou, J., Parrish,  
800 D. D., Wang, W., He, X., Cheng, C., Li, X. B., Yang, X., Song, Y., Wang, H., Qi, J.,  
801 Wang, B., Wang, C., Wang, C., Wang, Z., Li, T., Zheng, E., Wang, S., Wu, C., Cai, M.,  
802 Ye, C., Song, W., Cheng, P., Chen, D., Wang, X., Zhang, Z., Wang, X., Zheng, J., and  
803 Shao, M.: The formation and mitigation of nitrate pollution: comparison between urban  
804 and suburban environments, *Atmos. Chem. Phys.*, 22, 4539-4556, [10.5194/acp-22-](https://doi.org/10.5194/acp-22-4539-2022)  
805 [4539-2022](https://doi.org/10.5194/acp-22-4539-2022) 2022.

806 Yang, X., Wang, H., Lu, K., Ma, X., Tan, Z., Long, B., Chen, X., Li, C., Zhai, T., Li,  
807 Y., Qu, K., Xia, Y., Zhang, Y., Li, X., Chen, S., Dong, H., Zeng, L., and Zhang, Y.:  
808 Reactive aldehyde chemistry explains the missing source of hydroxyl radicals, *Nature*  
809 *Communications*, 15, 1648, [10.1038/s41467-024-45885-w](https://doi.org/10.1038/s41467-024-45885-w) 2024b.

810 Ye, C., Yuan, B., Lin, Y., Wang, Z., Hu, W., Li, T., Chen, W., Wu, C., Wang, C., Huang,  
811 S., Qi, J., Wang, B., Wang, C., Song, W., Wang, X., Zheng, E., Krechmer, J. E., Ye, P.,  
812 Zhang, Z., Wang, X., Worsnop, D. R., and Shao, M.: Chemical characterization of  
813 oxygenated organic compounds in the gas phase and particle phase using iodide CIMS  
814 with FIGAERO in urban air, *Atmos. Chem. Phys.*, 21, 8455-  
815 [8478,https://doi.org/10.5194/acp-21-8455-2021](https://doi.org/10.5194/acp-21-8455-2021) 2021.

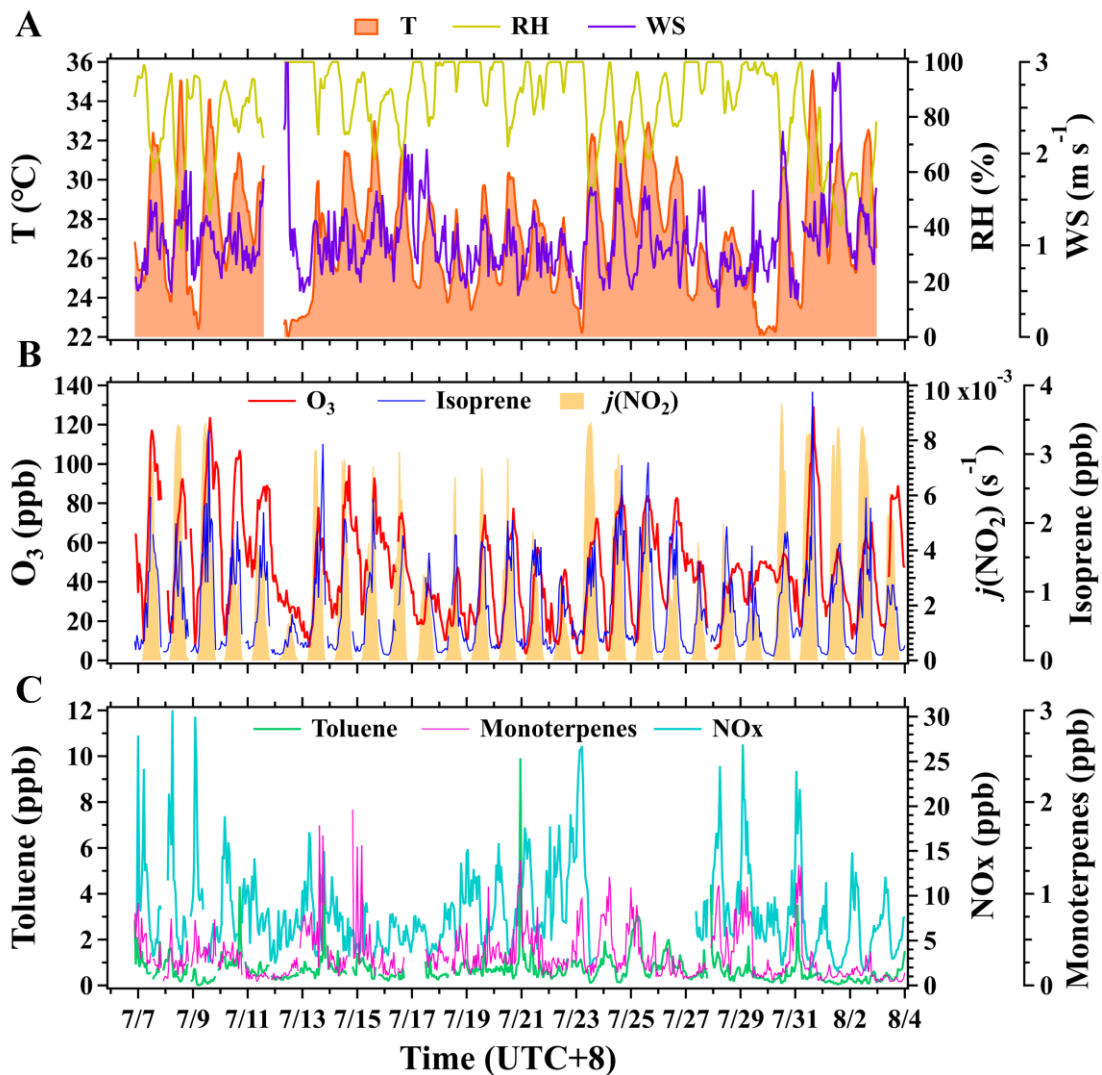
816 Yeo, M. J., and Kim, Y. P.: Long-term trends of surface ozone in Korea, *Journal of*  
817 *Cleaner Production*, 294, 125352, <https://doi.org/10.1016/j.jclepro.2020.125352> 2021.

818 Yuan, B., Koss, A. R., Warneke, C., Coggon, M., Sekimoto, K., and de Gouw, J. A.:  
819 Proton-Transfer-Reaction Mass Spectrometry: Applications in Atmospheric Sciences,  
820 *Chem Rev*, 117, 13187-13229, <https://doi.org/10.1021/acs.chemrev.7b00325> 2017.

821 Zhang, K., Xiu, G., Zhou, L., Bian, Q., Duan, Y., Fei, D., Wang, D., and Fu, Q.: Vertical  
822 distribution of volatile organic compounds within the lower troposphere in late spring  
823 of Shanghai, *Atmos Environ*, 186, 150-  
824 [157,https://doi.org/10.1016/j.atmosenv.2018.03.044](https://doi.org/10.1016/j.atmosenv.2018.03.044) 2018.

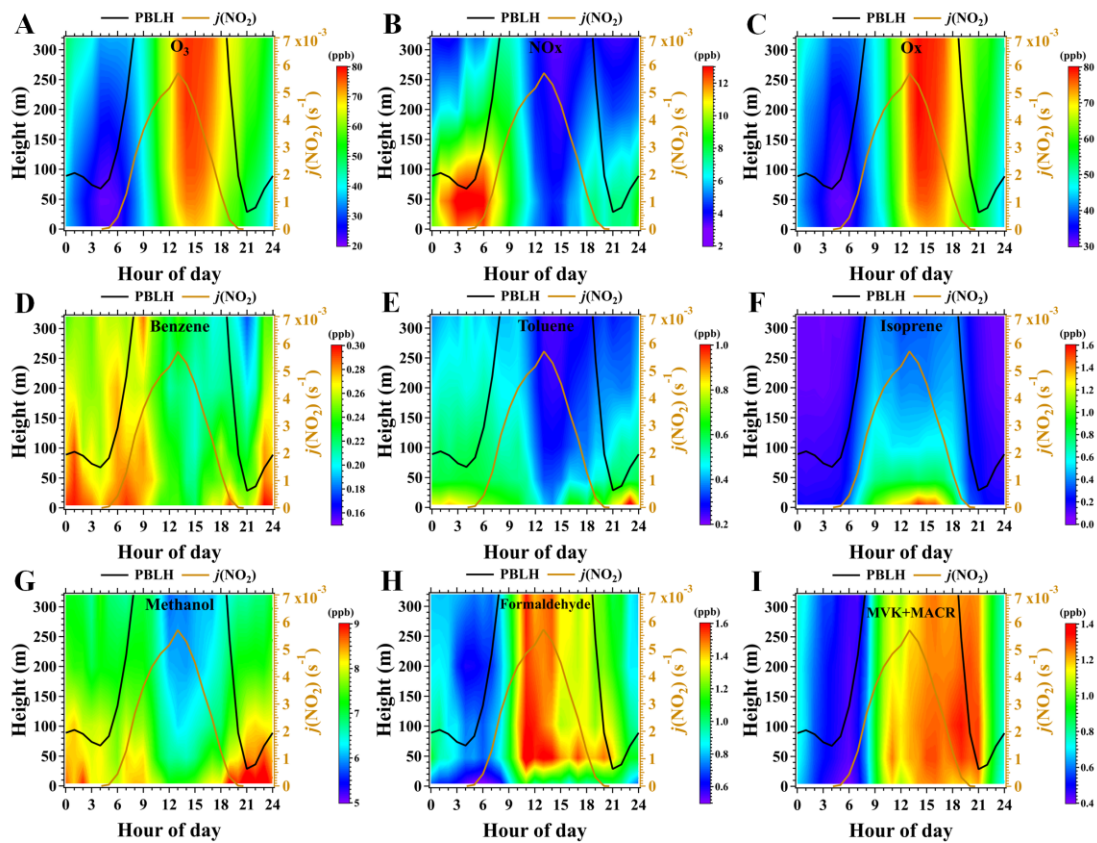
825 Zhang, Y., Xue, L., Mu, J., Chen, T., Li, H., Gao, J., and Wang, W.: Developing the  
826 Maximum Incremental Reactivity for Volatile Organic Compounds in Major Cities of  
827 Central-Eastern China, *Journal of Geophysical Research: Atmospheres*, 127,  
828 [e2022JD037296,https://doi.org/10.1029/2022JD037296](https://doi.org/10.1029/2022JD037296) 2022.

829 Zhao, M., Zhang, Y., Pei, C., Chen, T., Mu, J., Liu, Y., Wang, Y., Wang, W., and Xue,  
830 L.: Worsening ozone air pollution with reduced NO<sub>x</sub> and VOCs in the Pearl River Delta  
831 region in autumn 2019: Implications for national control policy in China, *J Environ*  
832 *Manage*, 324, 116327, <https://doi.org/10.1016/j.jenvman.2022.116327> 2022.



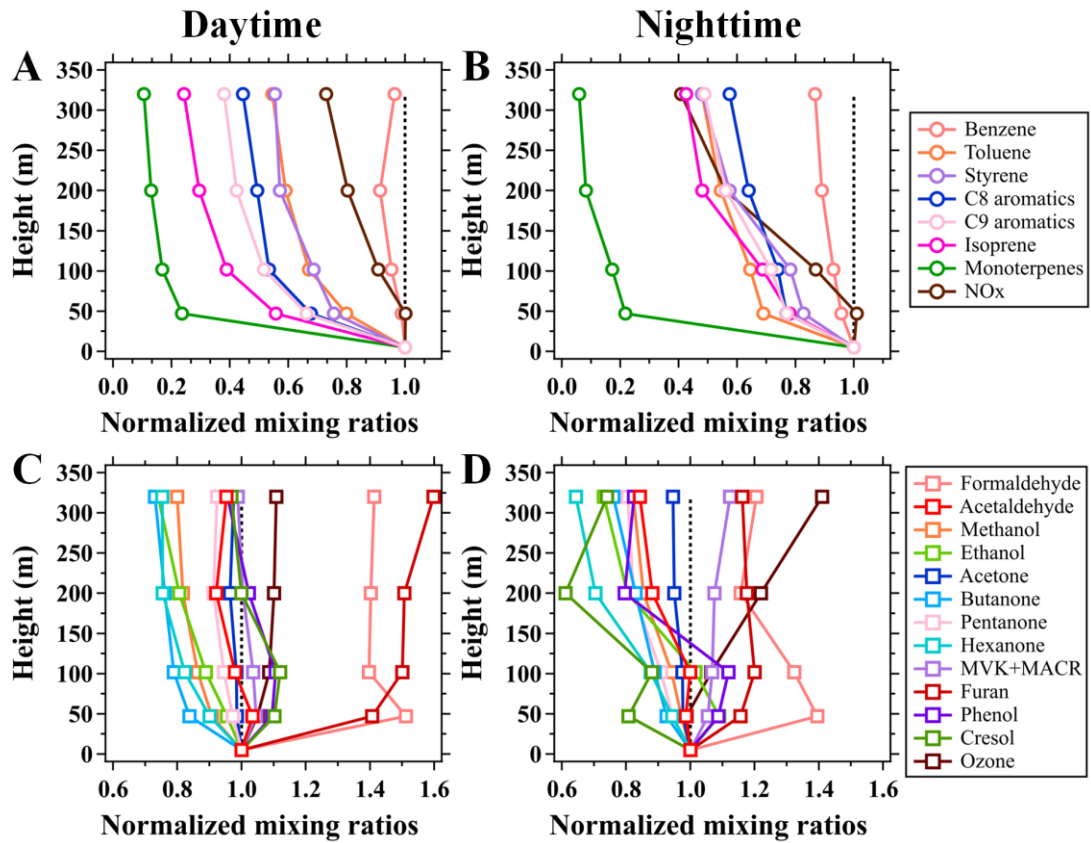
833

834 **Figure 1.** Time series of hourly mean air temperature (T), relative humidity (RH), wind  
 835 speed (WS), and mixing ratios of surface ozone, NO<sub>x</sub>, and VOC species along with  
 836  $j(\text{NO}_2)$  at the BMT site during the campaign. Meteorological parameters were measured  
 837 at 8 m above ground level and mixing ratios of ozone and its selected precursors were  
 838 measured at 5 m above ground level.



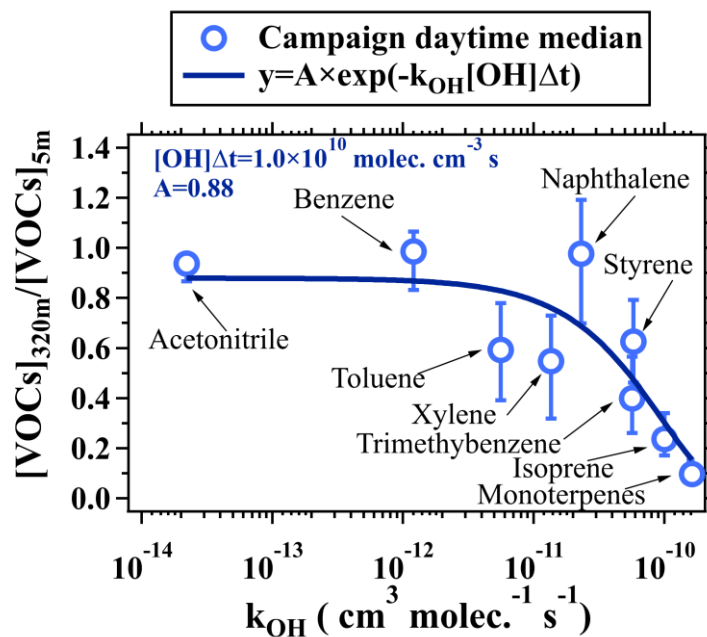
839

840 **Figure 2.** Average diurnal and vertical variations in mixing ratios ozone,  $\text{NO}_x$ ,  $\text{O}_x$   
 841 ( $\text{O}_3 + \text{NO}_2$ ), and six selected VOC species along with the average diurnal profiles of  
 842 PBLH and  $j(\text{NO}_2)$  during the campaign. The figures were obtained by linearly  
 843 interpolating the data at the five inlet heights on both altitude and temporal scales.



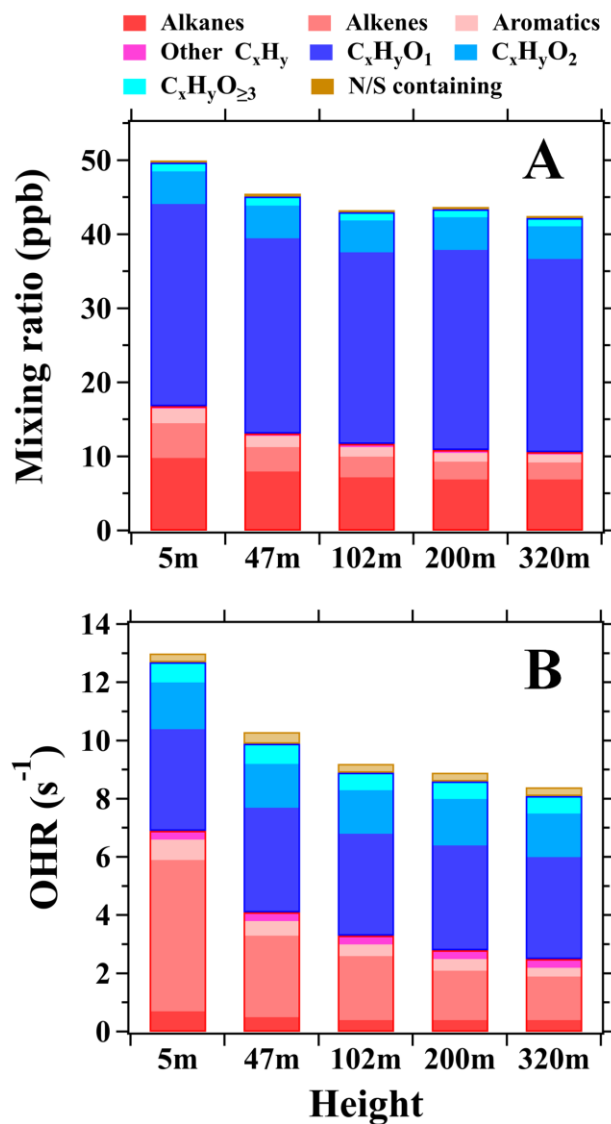
844

845 **Figure 3.** Average vertical profiles of (A-B) NMHCs and NO<sub>x</sub>, (C-D) OVOCs and O<sub>3</sub>  
 846 during the daytime (11:00-16:00 LT) and nighttime (23:00-04:00 LT) of the campaign.  
 847 The mixing ratios of the chemical species measured above 5 m are normalized to those  
 848 at 5 m.



849

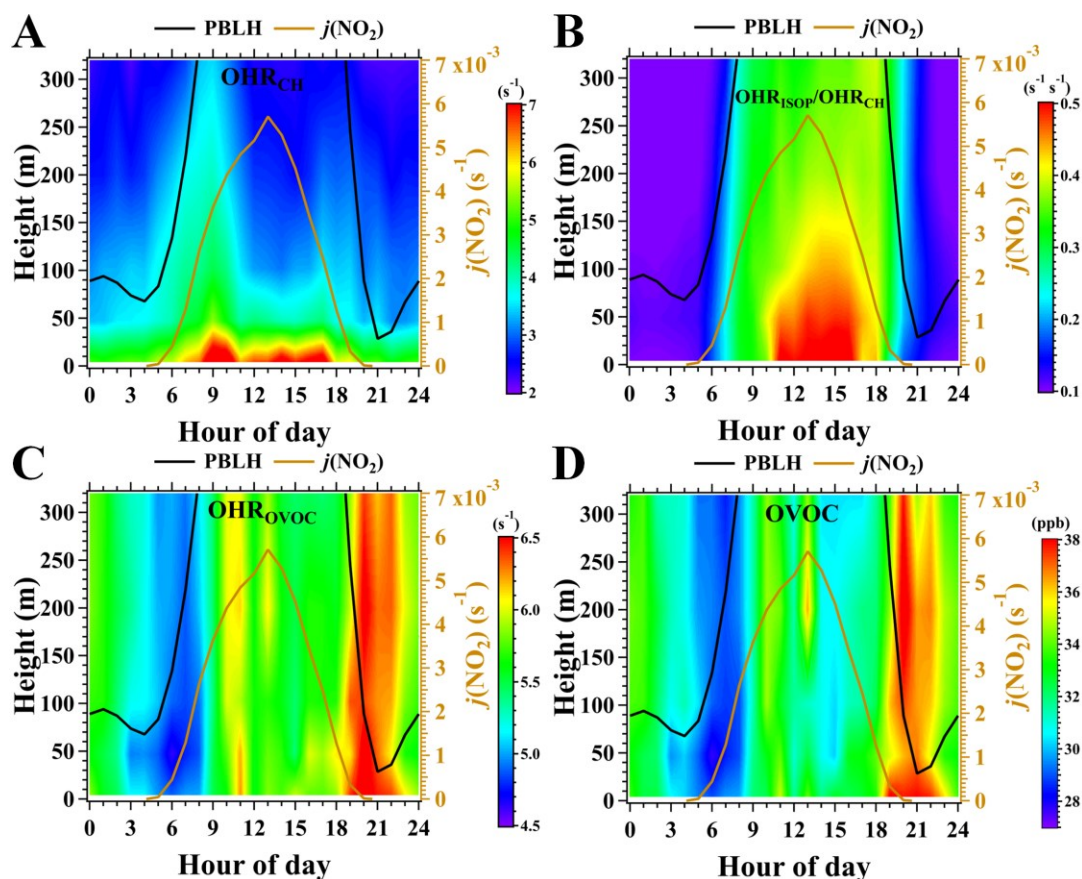
850 **Figure 4.** The change in ratios of NMHC concentrations (including acetonitrile)  
 851 between 320 m and 5 m as a function of  $k_{OH}$ . The vertically-resolved measurements of  
 852 VOCs made on the BMT in daytime during the campaign were used for analysis.  
 853 Hollow markers represent median values and error bars indicate the range between 25<sup>th</sup>  
 854 and 75<sup>th</sup> percentiles.



855

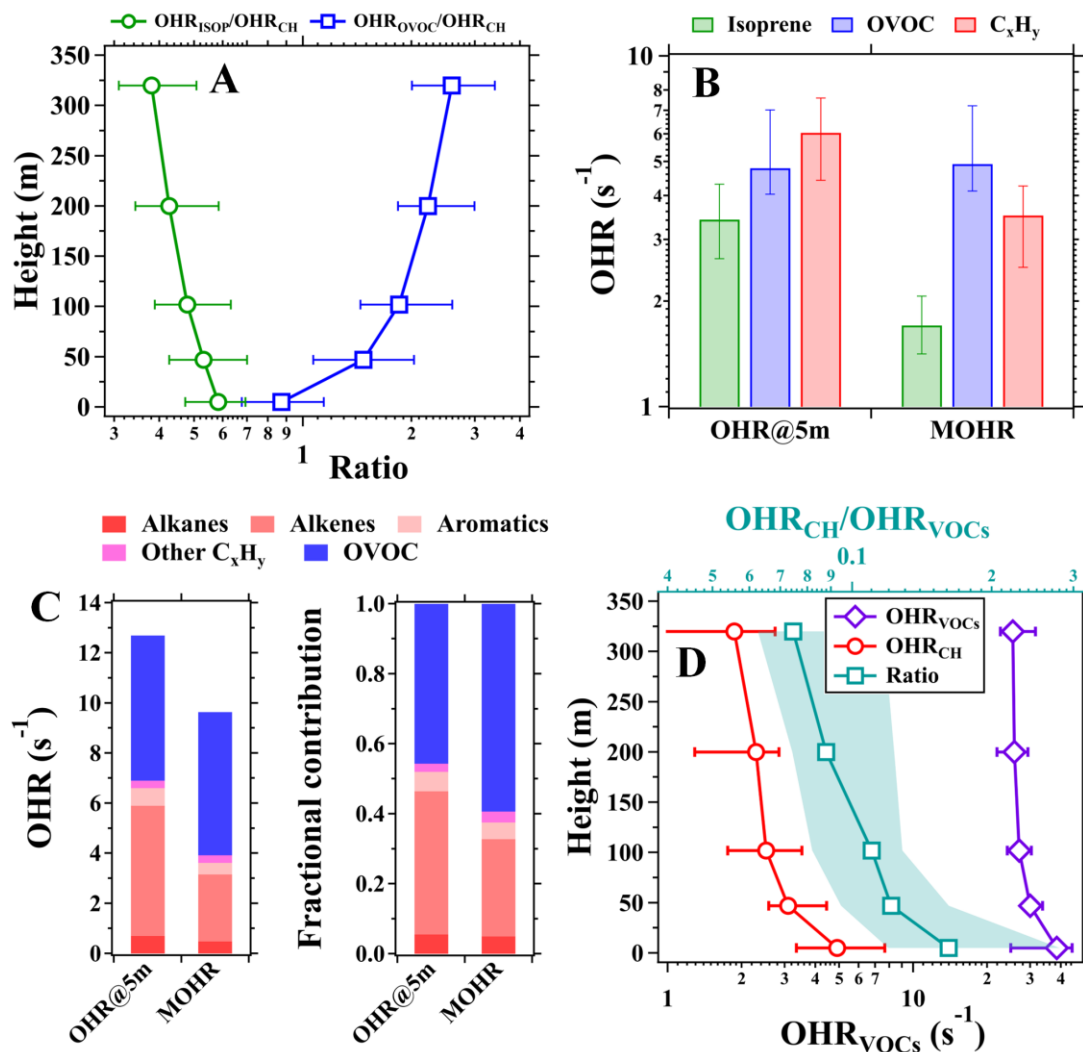
856 **Figure 5.** (A) Mean mixing ratios and (B) OHRs of different VOC categories at the five  
 857 inlet heights in daytime during the campaign.





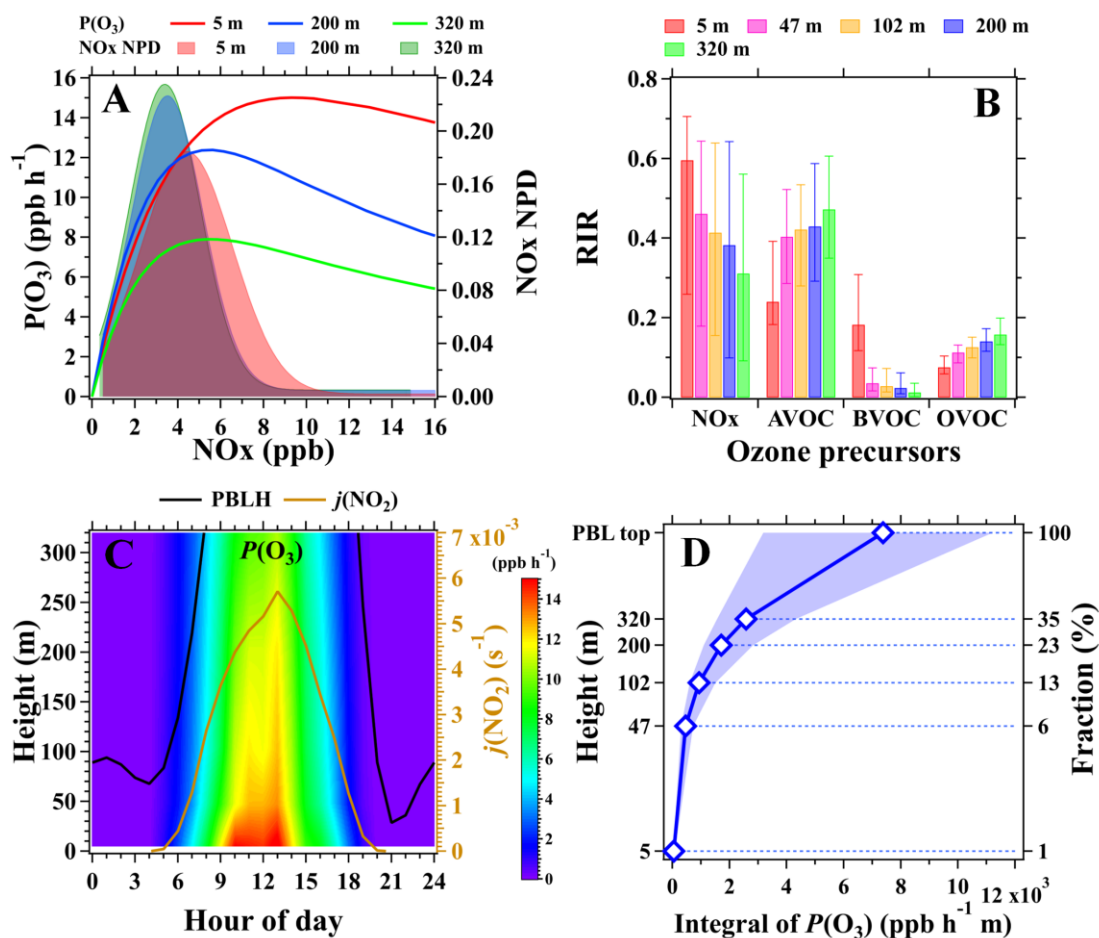
858

859 **Figure 6.** (A-B) Average diurnal and vertical variations in OHRs of  $\text{C}_x\text{H}_y$  and the OHR  
 860 ratios of isoprene to  $\text{C}_x\text{H}_y$  ( $\text{OHR}_{\text{ISOP}}/\text{OHR}_{\text{CH}}$ ) during the campaign. (C-D) Average  
 861 diurnal and vertical variations in mixing ratios and OHRs of OVOC. ISOP refers to  
 862 isoprene. The figures were obtained by linearly interpolating the data at the five  
 863 measurement heights on both altitude and temporal scales.



864

865 **Figure 7.** (A) Average vertical profiles of OHR ratios of isoprene to  $C_xH_y$   
 866 ( $OHR_{ISOP}/OHR_{CH}$ ) and OVOC to NMHC ( $OHR_{OVOC}/OHR_{CH}$ ). (B) Median values of  
 867 the OHR at 5 m and the mean OHR (MOHR) between 5 m and 320 m for isoprene,  
 868 OVOC, and  $C_xH_y$ . (C) Mean contributions of different VOC categories to the MOHR  
 869 below 320 m and the OHR at 5 m. (D) Vertical profiles of the measured  $OHR_{VOCs}$  and  
 870 the calculated  $OHR_{CH}$  (bottom axis) and the  $OHR_{CH}/OHR_{VOCs}$  ratios (top axis) during  
 871 July 28-31, 2021. The data used for analysis in panels A-D was within the time window  
 872 from 11:00 to 16:00 LT during the campaign. Markers in panels A and D represent  
 873 median values. Shaded areas and error bars in panels A, B, and D indicate the range  
 874 between 25<sup>th</sup> and 75<sup>th</sup> percentiles.



875

876 **Figure 8.** (A) Left axis: average dependence of  $P(O_3)$  on  $NO_x$  concentrations in  
 877 daytime during the campaign; Right axis: normalized probability density (NPD) of  
 878  $NO_x$  mixing ratios in daytime at the three inlet heights. (B) Median RIR values of  
 879 photochemical ozone formation to changes in  $NO_x$ , AVOC (NMHCs excluding BVOC),  
 880 BVOC (isoprene), and OVOC (nine OVOC species in Table S1) at the five inlet heights;  
 881 Error bars indicate the range between 25<sup>th</sup> and 75<sup>th</sup> percentiles. (C) Average diurnal and  
 882 vertical variations in  $P(O_3)$  during the campaign; The figure was obtained by linearly  
 883 interpolating the data at the five measurement heights on both altitude and temporal  
 884 scales. (D) The vertical profile of the integral of  $P(O_3)$  in daytime during the campaign;  
 885 Markers indicate median values and Shaded areas indicate the range between 25<sup>th</sup> and  
 886 75<sup>th</sup> percentiles.